

Spatial variability of dissolved cobalt in the Indian Ocean waters: Contrasting behavior in the Arabian Sea, the Bay of Bengal and the southern sector of the Indian Ocean

Nirmalya Malla^{1,2}, Sunil Kumar Singh*^{1,2}

¹CSIR National Institute of Oceanography, Dona Paula Goa.403004, India

² Academy of Scientific and Innovative Research (AcSIR), Ghaziabad- 201002, India

*Corresponding Author: sunil@nio.org

Abstract

The present study explored the dynamics of total dissolved Cobalt (dCo) in the Indian Ocean revealing different distribution patterns in the different sub-basins, nutrient-type in the southern sector, hybrid-type in the Arabian Sea to scavenged-type in the Bay of Bengal. The dCo in the coastal water of the Arabian Sea displays elevated (0.12-0.13 nmol/L) abundance and diminishes gradually towards the central Arabian Sea. Similarly, in the Bay of Bengal (BoB), dCo concentrations are notably higher in the northern region (0.11 nmol/L) gradually decrease towards south (0.03 nmol/L at 5°N). The Arabian Sea with higher biological uptake and remineralization in the oxycline supports a higher abundance of dCo in the intermediate oxygen minimum zone (OMZ), much a like the OMZs of the Atlantic and the Pacific Oceans. The influence of the phytoplankton community shift and uptake on the dCo distribution in the Indian Ocean could be inferred from the association between Co and phosphate in the photic waters. Our observation demonstrates scavenging type dCo profile in the BoB due to its higher riverine as well as dust inputs in addition to its supply from continental shelf sediments. Such higher concentration of dCo in surface waters of the northern BoB masks the dCo signal associated with nitrite maxima. dCo gets removed by its scavenging with Mn oxides at deeper depths as reflected by higher particulate Co in the BoB. Subduction fluid contribute significantly to the dCo inventory of the deep water in the Indian Ocean near Java-Sumatra subduction zone.

Plain Language Summary

Cobalt (Co) plays a significant role as a rare and vital bioactive trace metal essential for phytoplankton in the global ocean. The present study deals with the intricate biogeochemical processes of total dissolved Cobalt (dCo) in the Indian Ocean, comprising the Arabian Sea, the Bay of Bengal (BoB), and the southern sector of the Indian Ocean (30°S) and sheds light on the crucial sources of dCo as riverine input, atmospheric dust, continental shelf and Submarine Groundwater Discharge (SGD) to the surface waters whereas the Java- Sumatra subduction zone acts as a supplier of dCo to the deep waters. Though Arabian Sea OMZ waters have similar dCo cycling to the global ocean OMZ, the BoB shows a peculiar dCo distribution with surface maxima that is attributed to its large riverine, atmospheric and shelf sediment input to the surface water. Due to the intricate internal cycling of dCo with dissolved oxygen, the changing global climate and ocean deoxygenation will critically affect the dCo reservoir in the water column.

Key Points

- Rivers, atmospheric dust, continental shelf, and SGD supply dCo to surface waters.
- High dCo in deeper waters near the Java-Sumatra Subduction Zone could be due to release from the subduction zone.
- Contrasting internal cycling of dCo is observed in the Arabian Sea, the Bay of Bengal and the southern sector of the Indian Ocean.

Keywords: Dissolved Cobalt, Indian Ocean, GEOTRACES, OMZ, Climate change

1. Introduction

The Micronutrients are known to have significant impact on the ocean productivity as they act like metal enzymes for many of the metabolic reactions (Morel & Price, 2003). Cobalt (Co) is one among the important micronutrients with very low abundance in seawater limiting and co-limiting productivity in part of the global ocean (Bown et al., 2011; Chmiel et al., 2022; Hawco & Saito, 2018; Saito et al., 2002, 2004). Cobalt can substitute for Zinc (Zn) in the enzyme carbonic anhydrase in Zn-limited regions (Lane & Morel, 2000; Yee & Morel, 1996). Cyanobacteria, in particular *Prochlorococcus* Sp. and *Synechococcus* Sp., have an obligate requirement of Co for their growth that is distinct from other organisms (Hawco & Saito, 2018; Saito et al., 2002) because of their vitamin B12 or Cobalamin dependence that has cobalt as a metal centre. The vertical distribution of dCo has considerable significance as it reflects the dCo uptake by phytoplankton in the surface waters and its subsequent regeneration at the thermocline depth (Bown et al., 2011; Noble et al., 2012). Several sources have been identified as significant suppliers of dCo including riverine and estuarine input (Kharkar et al., 1968; Zhang et al., 1990), coastal sediments (N. J. Hawco et al., 2016; Noble et al., 2012, 2017), and to a lesser extent hydrothermal activities and the Aeolian dust (Noble et al., 2017; Shelley et al., 2012). However, the regeneration of dCo in the oxygen minimum zone (OMZ) in the water column and in the low-oxygen waters at the sediment-water interface in the coastal areas exert an important control on dCo budget (N. J. Hawco et al., 2016).

Though earlier studies characterised Co as a scavenging element (Whitfield & Turner, 1987; Nozaki, 1997), many recent studies confirmed its nutrient-type profile due to its drawdown by biological uptake controlling the distribution of dCo in the surface ocean (Saito et al., 2005; Saito and Moffett, 2002). Based on the modelling of large data sets produced since the commencement of GEOTRACES programme, cobalt seems to display hybrid-type profile in the global ocean (Tagliabue et al., 2018). Cobalt (Co) has a larger tendency to get scavenged with Manganese (Mn) due to their comparable ionic radii and redox potential, facilitating the incorporation of Co into bacterially produced Mn oxides rather than the non-biologically freshly made oxides (Cowen & Bruland, 1985; Moffett & Ho, 1996). A significant quantity of dCo is bound to strong organic ligands within the euphotic zone which increases its availability to phytoplankton impacting their ecology (Cowen & Bruland, 1985; Saito et al., 2010). Previous studies noted the presence of considerable amount of dCo in a labile and unbound state below the euphotic zone (Bown et al., 2012; Saito et al., 2005), hence suggesting that the cobalt is prone to scavenging (Moffett & Ho, 1996).

Measurements in several ocean transects for cobalt have been accomplished as a part of the international GEOTRACES initiative. Still, the scope of the observations remains confined to the

regional ocean basins especially in the Indian Ocean. Over the last decade, comprehensive observational data sets have been collected for the Atlantic Ocean, the Pacific Ocean, the Southern Ocean, the Arctic Ocean as well and the Mediterranean Sea suggesting continental margins, OMZs, atmospheric dust and rivers as the different sources of dCo which gives valuable insight into the dCo biogeochemical cycling (Dulaquais et al., 2017; Hawco et al., 2016; Noble et al., 2012, 2017; Chmiel et al., 2022; Bundy et al., 2020). However, the Indian Ocean is still relatively unexplored for dCo. The Indian Ocean is widely recognized as an extremely dynamic marine system due to its distinct physicochemical characteristics with the vast coastline associated with shelf margin, high riverine inputs in the BoB, huge atmospheric dust supply from the nearby deserts, Submarine Groundwater Discharge (SGD) along the coasts, and highly productive regions in the northern Indian Ocean that contribute to the uniqueness of the dCo biogeochemistry. Additionally, the presence of hydrothermal ridges and subduction zone at the Java- Sumatra region could be important sources of dCo in deeper waters, thereby impacting its budget. Besides, the presence of the OMZs in the northern Indian Ocean could make it a viable dCo reservoir highlighting its role in the dCo biogeochemistry. We measured the concentration of dCo in samples collected in the Indian Ocean including the Bay of Bengal, the Arabian Sea, and the southern sector of the Indian Ocean (up to 30 °S) onboard the GEOTRACES cruises GI09 and GI10. The current investigation elucidates the different sources of dCo in the Indian Ocean and their contrasting behaviour in the two OMZs of the Northern Indian Ocean, the Arabian Sea, the Bay of Bengal and the southern sector of the Indian Ocean, driven by their different physical and chemical properties adding knowledge to the dCo biogeochemical cycling.

2. Materials and Methods

2.1 Cruise track and Sampling

The seawater samples were collected from the Arabian Sea during January to February 2020 onboard cruise GI10 (SSD069, RV Sindhu Sadhana, Figure 1) whereas samples from the BoB, Andaman area, Southern sector of the Indian Ocean (up to 30 °S), and from the central Indian Ocean basin (CIOB) were collected on the cruise GI09 (SSD- 079, onboard RV Sindhu Sadhana) in the period of March - June 2021 (Figure1). Water samples were collected with 12L Teflon-coated Niskin X bottles (General Oceanics) using clean epoxy-coated 24-positioned rosette samplers deployed using KEVLAR hydro-wire (Chinni et al., 2018; Singh et al., 2020). Conductivity, temperature, depth, and salinity were measured using Sea-Bird CTD sensors. Seawater samples from 17 stations each were collected in the Arabian Sea during the cruise GI10, and similar number of stations were sampled during the cruise GI09. Water samples were collected in previously cleaned LDPE (Low-Density Polyethylene TARSONS) bottles. The bottles were cleaned following GEOTRACES protocol (Cutter et al., 2010);

first soaked in an alkaline solution (EXTRAN MA01), filled with Quartz distilled 2M HCl followed by 1M HNO₃ (Trace metal Grade- Fisher Scientific™). Samples were collected after these bottles were rinsed thoroughly with ultrapure water (18.2 Ωm Merck Millipore™) and packed in LDPE bags before sampling. The samples were sub-sampled from the Niskin X bottles by filtering through PALL Acropak™ Capsule filters of 0.22 μm pore size using filtered and compressed air. Sample bottles were rinsed thrice with respective seawater samples before collecting them. After collection, the samples were acidified using Optima grade HCl, (Fisher Scientific™) to maintain the pH of the sample <2, packed properly in the LDPE bags and brought to the laboratory at CSIR- National Institute of Oceanography for the trace metal analysis using the Sea-FAST HR-ICP-MS (Attom ES, Nu Instruments). The sub-sampling and acidification processes were performed under a class 100 laminar flow bench inside a class 10000 clean room customized inside a shipping container.

2.2 Measurements of Basic Oceanographic Parameters and Macro-nutrients

Physical oceanographic parameters like temperature, salinity, and Dissolved Oxygen (DO- Chemical Parameter) were measured using Sea-Bird CTD sensors. Fluorescence was measured using a Sea-Bird sensor (WET Labs ECO-AFL/FL) and Beam Attenuation was measured using another sensor (WET Labs C-star). The DO measurements in the cruise GI10 were obtained through the Sea-Bird CTD sensor whereas, the samples for the cruise GI09 were analyzed onboard collecting seawater and following the Winkler's Method. Macro-nutrients like silicate, phosphate, nitrate and nitrite were analysed in all samples collected during the cruises GI09 and GI10. For GI10 cruise, samples were frozen at -20°C and brought to CSIR-NIO Laboratory and nutrients measured using a spectrophotometer (SHIMADZU) whereas samples for GI09 were measured onboard using SKALAR Autoanalyser (Carritt & Carpenter, 1966; Winkler, 1888).

2.3 Analysis of Total Dissolved Cobalt

After the samples were brought to the laboratory, they were UV oxidized by an in-house UV-oxidation system. All the chemicals used for the trace metal analysis were high purity grade (Optima grade, Fisher Scientific™). Hydrochloric Acid (HCl), Nitric Acid (HNO₃), Acetic Acid (CH₃COOH), and Ammonia solution (NH₄OH) were used for making the working reagents. A mixed standard solution was prepared for the external calibration using Merck™ ICP single element standard solution (1000 ppm) and was diluted using Column Cleaned Sea Water (CCSW) to match the matrix of the seawater samples. The preparation of CCSW, standards, and the working of the sea-FAST HR-ICP-MS (Attom ES, Nu Instruments) were described in earlier publications of this group (Singh et al., 2020, 2023).

In addition to the external and internal calibration (using Rh), CCSW was run intermittently between samples as blanks. For each batch of analysis, freshly prepared CCSW is used as blanks. NASS-7 was run several times as a reference material to check the repeatability and reproducibility of the instrument. Along with NASS-7, two in-house standards were run and cross-checked with respect to the NASS-7. These two check standards (Chk-1 GI10/08-150 m and Chk-2 GI10/08-4500 m) were collected in bulk in precleaned 10 L LDPE cubitainers and were measured throughout the analysis. The measured concentrations of NASS-7 standard showed a very good concurrence with the reported values. The measured values of Co blanks, standards, NASS-7 are mentioned in Table S1 of the Supplementary Information. The measurement has an uncertainty of 1.07% with a detection limit of 0.0001ppb.

Samples from cross-over station were collected and analysed to validate the entire protocols of cleaning, sampling, and measurement of trace metals adopted in this study. Station ER05 (16.75 °N / 68.99 °E) sampled by the Japanese GEOTRACES program in 2009 (Vu & Sohrin, 2013) was re-sampled as cross-over station in this study in year 2020. A good correlation between the reported and measured values despite a gap of 12 years between the two samplings indicates a very good sampling and measurement protocols followed in this study (Figure S1).

3. Hydrography

Numerous studies have been conducted on the characterization of the water masses and their circulation pattern in the Indian Ocean (Murty et al., 1992; Schott & McCreary, 2001; Wyrski, 1973; You & Tomczak, 1993; You, 1997; Goswami et al., 2014). The Indian Ocean has low latitude land boundary in the northern part as the Arabian Sea and the Bay of Bengal are surrounded by continental land masses. Regardless of having almost the same latitudinal extent these two ocean basins have different characteristics in terms of their physical as well as chemical properties.

The surface water of the Bay of Bengal, Bay of Bengal Low Saline Water (BoBLSW), is characterized by very low salinity due to the large influx of fresh waters to the basin from the peninsular and the extra peninsular Indian Rivers as well as from Myanmar through Indo-Burman Ranges. The Ganga-Brahmaputra, Krishna, and the Godavari rivers contribute about 1.6×10^{12} m³ of fresh water annually to the BoB (Basu et al., 2001; Galy & France-Lanord, 2001; Sarin et al., 1989; Singh et al., 2008). This invasion of the low saline waters causes stratification in the water column. However, the presence of the warm as well as the cold core eddies helps break the stratification at some points (Madhupratap et al., 2003; Miriyala et al., 2017; Sarma et al., 2016). The Indian Ocean is also known as the link between the Atlantic and the Pacific Ocean where the warm surface waters from the Western Pacific Ocean

enter in large amounts via Indonesian islands and also through the Australian passage traced between 10 °S and 15 °S (Clemens et al., 2016; Frank et al., 2006; Song et al., 2004). Further moving southward, a more saline (> 35.5) and dense (25.4 Kg/m³) Subtropical Surface Water (SSW) formed due to excess evaporation over precipitation in the southern subtropical gyre of the Indian Ocean over 25 to 35 °S (Schott & McCreary, 2001; Wyrki, 1973) is present. Beneath the SSW, the water column is occupied by Sub Antarctic Mode Water (SAMW) south of 20 °S with a density range of 26.4-26.9 Kg/m³ and spreads over a depth of 200 to 800 m in the water column (You, 1998). This SAMW forms around 40 – 50 °S and brings oxygen-saturated water into the gyre at a temperature range of 6 -14 °C. In contrast to these high saline waters, Antarctic Intermediate Water (AAIW; You, 1998) with lower salinity is observed at a water depth of 800 – 1100 m in the southern sector of the Indian Ocean. In addition, the Modified North Atlantic Deep Water (MNADW) and the Antarctic Bottom Water (AABW) are occupying the bottom and deeper depths of the water column of the Indian Ocean. The MNADW results from the mixing of NADW and the CDW in the southern sector of the Indian Ocean occupying a water depth range of 2000 -3500 m whereas the AABW holds a depth below 3500 m in the water column (Dileep Kumar & Li, 1996; Goswami et al., 2014; Singh et al., 2012; You, 2000). MNADW originates in the southern Australian Basin and enters the Central Indian Ocean Basin (CIOB) through the Broken Plateau and South-East Ridge systems and the AABW enters the CIOB by the deep saddles present on the 90 °E ridge located at 5 °S and 10 °S (You, 2000). After entering the Indian Ocean, the MNADW continues to flow northwards whereas the bottom water bends and moves further southwards (Mantyla & Reid, 1995; Singh et al., 2020; Toole & Warren, 1993).

The Arabian Sea is characterized by the presence of the Arabian Sea High Saline Water (ASHSW), Persian Gulf Water (PGW), Red Sea Water (RSW), Modified North Atlantic Deep Water (MNADW), and Antarctic Bottom Water (AABW) (Dileep Kumar & Li, 1996; Goswami et al., 2014; Schott & McCreary, 2001; Singh et al., 2012; Wyrki, 1973; You, 2000). The surface water of the Arabian Sea, termed Arabian Sea High Saline Water (ASHSW), is formed due to excess evaporation over precipitation in the Arabian Sea region. The potential temperature falls in the range of 26±2 °C and the salinity ranges between 35.3 to 36.7 and is distributed uniformly over the Arabian Sea at a depth of 75 to 100 m. The PGW flows from the Persian Gulf via the Gulf of Oman and enters into the Arabian Sea having a characteristic potential temperature of 18 °C and salinity of 36.8 at its origin which drop to 12.5 °C and 35 respectively while traveling to the Arabian Sea (Shenoi et al., 1993). Likewise, the RSW originates from the Red Sea and flows at a depth range of 500 to 800 m spreading over the Arabian Sea and flowing further southwards. The surface water circulation is controlled by the seasonal reversal of the monsoonal winds over the Arabian Sea. This seasonality causes the emergence

of the East India Coastal Current (EICC) and West India Coastal Current (WICC) in the northern Indian Ocean resulting in an exchange of the surface waters between the Bay of Bengal and the Arabian Sea. In the winter monsoon period, the North Monsoon Current (NMC) has a profound influence over the Arabian Sea as it brings the low saline BoB waters into the Arabian Sea that is observed at stations GI10/4 and 5 (Figure. 2). In addition, the southeastern boundary of the Arabian Sea experiences mesoscale eddies migrating westward (Bruce et al., 1998; Rao et al., 2013; Shankar & Shetye, 1997). The invasion of the low-saline BoB waters causes intense baroclinic instability which further results in the meandering of NMC and the formation of anticyclonic eddies (Rao et al., 2013) and westward dispersion. This phenomenon is observed as a decrease in salinity from 35.45 at GI10/10 to 35.16 at GI10/11 along with the shoaling of potential density anomalies in the region (Figure 2).

4 Results

4.1 Macronutrients and Dissolved Oxygen

The surface DO concentration varies between 200 and 240 μM and decreases gradually with depth and further increasing under the influence of deeper waters (below 1000 m). The DO decreases down to 5 μM (100-1000 m) prevailing suboxic conditions in the Northern Indian Ocean (Arabian Sea and BoB). In a few regions, the DO falls as low as near zero forming anoxic zones in the Arabian Sea further leading to the formation of denitrification zones. The on-board measured DO in the track of GI09 is shown as section plot (Supplementary Figure. S2). However, due to some technical issues we were unable to measure the DO at some of the stations of the track GI10 in the Arabian Sea, data acquired at some stations are mentioned in the supplementary information.

The macronutrients i.e., silicate (Si), phosphate (PO_4^{3-}), nitrate (NO_3^-) and nitrite (NO_2^-) were also measured throughout the water column along the cruise track of GI09 onboard using the SKALAR Autoanalyser. Along the track of GI10 in the Arabian Sea, Silicate, Phosphate and nitrite were measured but the nitrate could not be measured due to some technical problem in the experimental setup. Surface concentrations of these nutrients show a minimum due to biological uptake. The values go as low as 0.1 μM for PO_4^{3-} , <5 μM for Si, and <1 μM for NO_3^- . This surface low persists up to 150 – 200 m and then starts increasing to a maximum at the depth of 800 – 1000 m in the case of PO_4^{3-} and NO_3^- and 2000 to 2500 m for Si with values of 3.4 μM , 38 μM , and 160 μM respectively in the Indian Ocean (Figure. S3, S4, S5). These values remain more or less constant in the deeper waters. The measurement of nutrients in samples of the cruise GI09 was validated by measuring MOOS-3 reference material with a consensus value of less than 10% uncertainty.

4.2 Total Dissolved Cobalt (dCo)

4.2.1 dCo in the Arabian Sea

dCo abundance in the water column of the Arabian Sea has a range of 0.015-0.15 nmol/L. The coastal water of the Arabian Sea displays a greater concentration of dissolved cobalt of 0.12-0.13 nmol/L in the surface waters and ~0.06 nmol/L in the bottom waters (GI10/01 and 02; Figure 3a and 4a). The high surface concentration of dCo gradually decreases to ~0.02 nmol/L while approaching the open ocean waters. dCo in the perennial OMZ region of the eastern Arabian Sea has comparatively higher surface values of 0.037-0.05 nmol/L (GI10/17 and 18).

The dCo concentration gets its maximum value around 100-150 m water depth reaching 0.05-0.06 nmol/L in the open ocean waters and even higher (0.075-0.115 nmol/L) (GI10/17 and 18) in the perennial OMZ region of the Eastern Arabian Sea. Further, a fall in the concentration up to 0.015-0.03 nmol/L is observed in the deeper parts of the water column (Figure 3a and 4a). Overall, the dCo displays hybrid-type behavior in the Arabian Sea (Figure 4a).

4.2.2 dCo in the Bay of Bengal

The dCo in BoB ranges from 0.02 to 0.11 nmol/L. Surface dCo in the BoB shows higher values of 0.09-0.11 nmol/L which decreases gradually up to 0.02 nmol/L in the deeper waters (GI09/02; Figure 3b and 4b). The profile of dCo in the open ocean is somehow special. It does not show the typical hybrid-type of profile rather it shows a scavenging-type of profile (Figure 4b). In addition, the OMZ waters of the BoB show a marginally increasing trend of dCo up to ~0.035 nmol/L (GI09/02). Coastal BoB has an overall higher range of dCo ranging from ~0.1 nmol/L in the surface to ~0.025 nmol/L at 80 m depth which further increases with depth up to 0.060 nmol/L at the bottom (Figure 3b and 4b).

The high surface concentration of dCo decreases gradually moving southward from the Northern Indian Ocean. The surface high dCo of 0.11 nmol/L in the Northern Indian Ocean decreases to < 0.03 nmol/L in the equatorial Indian Ocean at 5 °N latitude (GI09/05) and even lower further south. In the deep water of the Java-Sumatra Subduction Zone area, there is an enrichment of dCo as high as 0.05-0.065 nmol/L (GI09/05, 3300 – 4250 m; Figure 3b and 4c).

4.2.3 dCo in the Southern Sector of the Indian Ocean and Central Indian Ocean Basin

The overall dCo in the southern sector of the Indian Ocean (30 °S; GI09/14-16) is lower (<0.04 nmol/L) compared to its northern counterpart (Figure 3b and 4d) and display nutrient-type vertical profile (Figure 4d). The surface concentration of dCo varies in the range of 0.002 to 0.01 nmol/L which persists up to 100 m. The dCo concentration increases up to 0.03-0.04 nmol/L below 800 m with a

subsequent decrease to around 0.01-0.02 nmol/L further downward. Despite the presence of the South-East and South-West Indian Ridges in the southern sector of the Indian Ocean, hydrothermal signatures of dCo were not traced in this region.

In the Central Indian Ocean basin, the surface dCo remains in the range of 0.015-0.025 nmol/L, however, a slight increase in the concentration of 0.08-0.095 nmol/L is observed at GI09/ 21 around water depth of 75 – 100 m (Figure 3b and 4f). The deep-water concentration of dCo lies in a range of 0.01-0.02 nmol/L.

5. Discussions

5.1 Distribution of dCo in surface waters

The surface distribution of dCo exhibits a significant degree of variability within the Indian Ocean, from 0.002 nmol/L to 0.13 nmol/L (Figure 5). This variability is observed across many regions within the Indian Ocean, including the Arabian Sea, Bay of Bengal (BoB), Central Indian Ocean Basin (CIOB), and the southern sector of the Indian Ocean (SIO). The concentration of dissolved cobalt displays an increasing trend from the southern sector of the Indian Ocean towards the Northern Indian Ocean. Notably, the coastal Bay of Bengal (BoB) records a maximum concentration of 0.11 nmol/L, whereas the eastern coastal Arabian Sea reaches an even higher concentration of 0.130 nmol/L. Elevated values observed in coastal regions may be attributed to significant contributions from atmospheric dust deposition, riverine influx, and submarine groundwater discharge along with contribution from shelf sediments.

Despite having a significantly enhanced abundance of dCo in the coastal BoB and the Arabian Sea, the depth profiles of dCo in their water columns are quite different (Figure 4). The Arabian Sea exhibits a characteristic hybrid-type water column profile similar to most of the global ocean basins (Chmiel et al., 2022; N. J. Hawco et al., 2016), however, in contrast, the Bay of Bengal (BoB) displays a scavenging-type of profile (GI09/02). The surface high of dCo in BoB has a resemblance to the Arctic shelf and the Gulf of Alaska (Bundy et al., 2020; Chmiel et al., 2022). The presence of a surface high in the Bay of Bengal (BoB) can be attributed to significant riverine input originating from the Ganga-Brahmaputra riverine systems (Robinson et al., 2007; Sengupta et al., 2006) or shelf input (Noble et al., 2012, 2017). Apart from the riverine input, atmospheric dust has been identified as a significant source of dCo in the Northern Indian Ocean (Chester et al., 1991; Srinivas & Sarin, 2013), as it receives a substantial amount of dust from the Saharan desert, Arabian desert, and nearby regions, Thar desert as well as from the Indo-Gangetic Plains and the Peninsular India (Aswini et al., 2020; Bikkina et al., 2023; Chester et al., 1991; Karri et al., 2024; Kumar et al., 2012, 2020; Srinivas & Sarin, 2013; Tindale

& Pease, 1999). Overall concentration of dCo in the southern sector of the Indian Ocean is low (Figure 4) and it displays nutrient type profile. Lack of external sources maintains the lower concentration of dCo in the surface waters in this region.

5.2 Significant sources of dCo to the surface waters of the Indian Ocean

Atmospheric input could be a crucial source of several micronutrients to the surface ocean waters. In the present study, the atmospheric flux (both dry and wet deposition) of soluble Co to the Indian Ocean has been estimated (Supplementary Text S1) using model-based soluble Al deposition fluxes (Xu & Weber, 2021) (Figure S6). The spatial map of atmospheric deposition of Co (Figure S6) displays the highest soluble Co in the Eastern Arabian Sea, reaching up to $4.5 \mu\text{mol m}^{-2} \text{yr}^{-1}$ in the present study area. A considerable difference in the atmospheric Co fluxes between the Arabian Sea ($4.5 \mu\text{mol m}^{-2} \text{yr}^{-1}$) and BoB ($\sim 1-1.5 \mu\text{mol m}^{-2} \text{yr}^{-1}$) is observed due to the higher soluble Al flux in the Eastern Arabian Sea indicating a huge continental source. This feature is also observed for the soluble Mn (Singh et al., 2023). This could be due to high dust input from Peninsular India during the NE Monsoon and/or wet deposition during the summer monsoon (Figure S7; Kumar et al., 2012; Suresh et al., 2021). The Deccan Basalt and the Southern Granulitic Terrain of Peninsular India with Co concentrations in the range of 28 to 63 and 0.6 to 72 $\mu\text{g/g}$ respectively seem to be the crucial dust sources contributing to the high soluble Co in the Eastern Arabian Sea (Laxman et al., 2022; Yellappa & Rao, 2018). The combined average dust input in the BoB and the Arabian Sea (11.3 Mmol/yr) constitutes the 17% of the global dust input (Tagliabue et al., 2018). In addition, dust sources from the desert regions of Saudi Arabia and Northern Africa enhance the soluble Co flux in the western Arabian Sea. Further south, the soluble Co flux decreases to $0.1-0.5 \mu\text{mol m}^{-2} \text{yr}^{-1}$. A decrease in the soluble Co flux towards the southern sector corresponds to the lower continental dust contribution in the southern Indian Ocean, except for a minor increase in the eastern TSIO ($\sim 0.5 \mu\text{mol m}^{-2} \text{yr}^{-1}$) under the influence of the Australian dust (Karri et al., 2024).

The Northern Indian Ocean receives a large influx of fresh water and sediments from several large rivers carrying huge amounts of micronutrients to the surface waters of the Northern Indian Ocean. Three major rivers, the Indus, the Narmada, and the Mahi debouches a total freshwater discharge of $272.78 \text{ km}^3 \text{yr}^{-1}$ into the Arabian Sea whereas a total water discharge of $1587.85 \text{ km}^3 \text{yr}^{-1}$ is estimated in the BoB via the major rivers like the Ganga- Brahmaputra, the Irrawaddy, the Mahanadi, the Damodar, the Godavari, the Krishna and the Cauvery (Gupta et al., 2022; Milliman & Meade, 1983; Sarin et al., 1989). These rivers could be potential sources of dCo to surface waters in the BoB which is confirmed by the dCo in MLD (Mixed Layer Depth) vs salinity plot deciphering a high dCo at low salinity (Figure S8). A significantly high dCo concentration in the Hooghly river, 0.8 nmol/L , was

reported (Samanta & Dalai, 2018). Additionally, dCo could be contributed by its desorption from sediments in the estuarine region (Samanta & Dalai, 2018). The total riverine discharge of dCo including desorption from sediments in the estuary to the surface waters of BoB is estimated to be 2.27 Mmol annually. Similarly, by considering the total riverine discharge to the Arabian Sea and dCo concentration at zero salinity (0.85 nmol/L of the Narmada river); (Mishra & Kumar, 2020), the total flux to the Arabian Sea is estimated as $\sim 0.23 \text{ Mmol yr}^{-1}$ ($\sim 0.06 \mu\text{mol m}^{-2} \text{ yr}^{-1}$). The total estimated riverine flux in NIO constitute $\sim 43\%$ of the global riverine dCo flux (Tagliabue et al., 2018). Variations in the riverine input might have been observed during monsoonal changes for which a seasonal observation is required.

In addition to the atmospheric and riverine inputs, the Submarine Groundwater acts as another source for the dCo to the surface waters of BoB. The submarine groundwater discharge (SGD) is reported to be $333.4 \text{ km}^3 \text{ yr}^{-1}$ and $200 \text{ km}^3 \text{ yr}^{-1}$ in the BoB and Arabian Sea respectively (Damodararao & Singh, 2022; Prakash et al., 2021; Rahaman & Singh, 2012; Samanta & Dalai, 2018). Considering $\sim 5\%$ fraction of it to be freshwater (Damodararao and Singh, 2022) and the average dCo concentration in the groundwater to be 6.2 nmol/L (Samanta & Dalai, 2018), the SGD flux is calculated to be $0.103 \text{ Mmol yr}^{-1}$ ($0.047 \mu\text{mol m}^{-2} \text{ yr}^{-1}$) in the BoB. However, average dCo concentration in the aquifers of the west coast is taken as $\sim 1.08 \mu\text{g/L}$ (18 nmol/L) (Akshitha et al., 2022) and $\sim 15\%$ fraction of fresh SGD (Lino et al., 2023), the SGD flux in the Arabian Sea is estimated to be 0.54 Mmol/yr ($0.14 \mu\text{mol m}^{-2} \text{ yr}^{-1}$).

5.3 dCo in the deeper waters of the Indian Ocean

The dCo in the deeper waters of the Indian Ocean shows large spatial variability, ranging from 0.005 nmol/L to 0.064 nmol/L (Figure 3a and b). Close to the Java-Sumatra Subduction Zone (GI09/05), the dCo exhibits a rising trend, reaching a maximum of 0.064 nmol/L at a depth of 4250 m (Figure 3b and 4c). The persistent increasing pattern of dCo concentrations at depths below 3000 m in the subduction zone renders it a probable origin of dCo in these deeper waters. The Indian Plate subducting beneath the Eurasian Plate facilitates the transport of the metal-rich seafloor sediments (Pattan et al., 2017) of the Central Indian Ocean which is enriched with Cu, Ni and Co along with Fe and Mn (Valsangkar et al., 1992). The interaction of the recirculated seawater through the faults of the trench with the polymetallic nodule rich crust could probably a reason for the release dCo along with other trace metals to the deeper water column as it has been found in the case of dFe (Chinni et al., 2018). The higher $\delta^3\text{He}$ ($\sim 15\%$) data nearby this region also confirms the presence of mantle sourced materials in the deeper waters (Srinivasan et al., 2004). Apart from this the dCo values of 0.064 nM in GI09/05 near the trench and further decreasing to 0.038 nM at GI09/06 marginally away from the trench region at a

depth below 4000 m also adds to aforementioned discussions. This enhancement in dCo in the subduction zone is further confirmed by the higher beam attenuation coefficient signal measured by the Sea-Bird Sensor (WET Labs C-Star) (Figure S9). This source of dCo is distinct and limited to the deeper waters of the Indian Ocean and has not been documented yet from other oceanic regions.

However, the present study does not show any signature of Hydrothermal release of dCo from the active spreading ridges of the Indian Ocean. dCo concentration around the known ridges, the Southeast Indian Ridge (station GI09/15) and the Carlsberg Ridge (GI10/14) are similar to their background level (Figure. 3a and b). Though the global dCo budget estimate suggests a flux of 2×10^6 mol/yr to the deep waters via hydrothermal vents constituting $\sim 2.4\%$ of the total marine Co budget (Swanner et al., 2014), recent studies (N. Hawco et al., 2018) estimate it to be $\sim 0.3\%$. Very few hydrothermal vents are reported to be a source of dCo, for example, the Loihi Seamount in the Pacific Ocean (Chmiel et al., 2022). The dCo has not been reported to travel very far distances from its hydrothermal vents as the labile Co particularly is prone to scavenging indicating immediate precipitation of dCo near the hydrothermal vents with a local vertical transport of dCo in the surrounding water column rather than the horizontal transport (Chmiel et al., 2022). In the present study the unavailability of any dCo signature like dMn or dFe near the Carlsberg Ridge, SEIR, or the Central Indian Ridge (Chinni et al., 2018; Nishioka et al., 2013; Ray et al., 2012, 2020) could be due to the distance of the sampling sites from the vent site.

5.4 Relationship of dCo with Phosphate and DO:

The distribution of dCo in the open ocean shows a hybrid profile, with the highest concentration occurring in the oxycline (Chmiel et al., 2022; N. J. Hawco et al., 2016). In our study, we have observed correlations between dCo, phosphate (PO_4^{3-}), and dissolved oxygen (DO) at various depths in the Bay of Bengal (BoB), Arabian Sea (Figure 6 a-h). Further, we have plotted the representative dCo profile along with DO, phosphate, nitrate and nitrite at different regions of the Indian Ocean (Figure 7) for better comparison. Throughout the water column of the Indian Ocean, dCo seems to correlate with PO_4^{3-} and DO differently in different sub-basins (Figure 6 a-h). In the Arabian Sea (other than coastal ocean), the positive correlation between dCo and PO_4^{3-} suggests their uptake by marine organisms in the surface waters due to high productivity, followed by its release in the deeper waters due to remineralization (Figure 6a).

Further below the oxycline, there is a decrease in dCo compared to PO_4^{3-} , indicating scavenging of dCo in deeper waters. Additionally, the inverse relation with DO in the top 250 meters confirms the release of dCo in low oxygen conditions in the Arabian Sea due to remineralization and organic matter

respiration (Figure 7b). Below 250 meters, there is a gradual decrease in dCo, suggesting the dominance of the scavenging process over biotic uptake and remineralization. Coastal samples with very high dCo and low surface PO_4^{3-} do not confirm the biological uptake and remineralization pattern, likely due to high input from external sources, from atmospheric input and shelf sediments (Figure 6a). In the BoB, dCo exhibits a scavenging nature in the upper 250 meters in both coastal and open ocean waters. The inverse trend with PO_4^{3-} in the BoB suggests the dominance of scavenging over biological uptake (Figure 6c), and the decrease of dCo with DO in the top 250 meters further confirms the dominance of scavenging over release due to remineralization and organic matter respiration (Figure 6d and Figure 7b). Interestingly, dCo in the BoB correlates with the PO_4^{3-} in the deeper waters, suggesting its remineralization with PO_4^{3-} at deeper depths (Figure 6c and 7b). Such an association between dCo and PO_4^{3-} has been observed previously in the BoB (Ikhsani et al., 2023). The remineralization of dCo with respect to PO_4^{3-} in the OMZ region of BoB has been observed at deeper and marginally longer length scales compared to the Arabian Sea (Figure 6c) which could be explained by the ballast effects in the presence of a large amount of lithogenic particles in the BoB brought by the Ganga-Brahmaputra riverine system increasing the sinking speed of aggregates and the depth of remineralization (Rixen et al., 2019). The Ballast effect is known as the coagulation of the organic matter with the lithogenic particles thereby increasing the speed of the sinking of the aggregates through the water column so as increasing the depth of remineralisation (Ittekkot & Haake, 1990; Kwon et al., 2009).

In the Southern Sector of the Indian Ocean (SIO) and the Central Indian Ocean Basin (COIB), euphotic waters (0-250m), dCo show a positive correlation with PO_4^{3-} with p value <0.001 , indicating biotic uptake of dCo and subsequent remineralization (Figure 6e and 6g) and further decrease in dCo with an increase in PO_4^{3-} in the deeper waters, indicating a scavenging process (Figure 6e, g) as has been suggested in earlier studies in the Atlantic and Pacific oceans (Chmiel et al., 2022; Hawco et al., 2016). However, the p-value for the deeper depths is >0.01 indicating the correlation between dCo and PO_4^{3-} at deeper depths in these regions are not highly significant. The correlation with DO is weaker at SIO as compared to other parts of the Indian Ocean. The overall correlation between dCo and DO throughout the water column shows a stronger association in the Arabian Sea, likely due to intense remineralization of organic matter and corresponding oxygen utilization.

The dCo also demonstrates a significant association with phosphate (PO_4^{3-}) in the euphotic zone on a global scale due to surface biological uptake by the phytoplankton and subsequent remineralisation of dCo along with the phosphate (Bown et al., 2011; Ellwood, 2008; Noble et al., 2008; Saito et al., 2010; Saito et al., 2004, 2017; Saito & Moffett, 2002). The dCo and PO_4^{3-} correlation in the Atlantic Ocean

demonstrates an average Co:P slope of $23.1 \mu\text{M M}^{-1}$ with variations in the regional scale ($21.5\text{-}65.8 \mu\text{M M}^{-1}$; (Dulaquais et al., 2014)). These observed variations in the Co:P slope in different biogeochemical domains within the same ocean could be linked to the different phytoplankton assemblages. Additionally, other factors such as the differential surface regeneration rate of various ecosystem species, differential input of dCo from various sources, and physical processes could influence the Co:P slope regionally (Noble et al., 2008). The current study demonstrates variations in the Co:P slope in different regions of the Indian Ocean, potentially attributed to the existence of specific phytoplankton communities (Figure 8a-e). The slope of Co:P progressively rises from 18 to $41 \mu\text{M M}^{-1}$ from the Southern Sector of the Indian Ocean to the Northern Indian Ocean (Arabian Sea perennial OMZ; Figure 8). The northward increase in the Co:P slope in the Indian Ocean infers the enhanced biological uptake of dCo in the Northern Indian Ocean. Even, within the Arabian Sea, different slopes indicate the shift in the phytoplankton community. The enriched bacterial community and *Synechococcus* in the perennial OMZ area (Eastern Arabian Sea) and also seasonal *Trichodesmium* bloom (Garrison et al., 2000; Matondkar et al., 2006) enhance the dCo uptake making Co:P slope steeper as the cyanobacteria has higher demand for the dCo. Furthermore, the lower intercept (Figure 8) in the Eastern Arabian Sea, which accounts for the leftover dCo after biological consumption, confirms the higher dCo uptake due to enhanced productivity and high uptake rate due to shift in the microbial community. The phytoplankton community in the BoB is predominantly composed of *Prochlorococcus* and *Synechococcus* accounting for 66% of the community population (Sarma et al., 2016). However, it is noteworthy that the slope of Co:P differs significantly from that observed in the other regions of the Indian Ocean. The negative slope ($-27 \mu\text{M M}^{-1}$) indicates the enrichment of dCo in the surface waters of the BoB by multiple potential sources and the limited influence of biological factors on the dCo distribution (Figure 8). The low productivity and subsequent low biological utilization along with high input from dust, river, and SGD contribute to a negative correlation between the dCo and PO_4^{3-} . This can be further confirmed by the particulate Co (pCo) and Phosphate (pP) (Weisend, 2017) in the BoB region which portrays the decoupling between surface pCo and pP. This unique characteristic sets the BoB apart from the other regions of the Indian Ocean in terms of dCo distribution.

5.5 Contrasting biogeochemical behavior of dCo between the Bay of Bengal, the Arabian Sea and the southern sector of the Indian Ocean

Different parts of the world ocean show a typical hybrid dCo profile including the OMZ regions (Chmiel et al., 2022; N. J. Hawco et al., 2016; Noble et al., 2017). The present study displays dCo trend in the OMZ waters of the Arabian Sea similar to other global OMZ (N. J. Hawco et al., 2016).

However, it is noteworthy that the Bay of Bengal (BoB), despite possessing an OMZ, exhibits a different vertical distribution. Further, the southern sector of the Indian Ocean display nutrient-type profile for dCo with overall lower concentration. In the Arabian Sea, the dCo profile shows a surface low commonly attributed to the biological uptake of dCo, followed by remineralisation that manifests a peak in the oxycline that corresponds to the secondary nitrite maxima (Figure 9, 10a). Further, the observed trend of a progressive decline in dCo with depth corresponds to the oxidation of Co (II) along with the Mn by biologically mediated oxidation. This can be understood in terms of the observed dMn peak and the corresponding nitrite peak in the OMZ of the Arabian Sea (Singh et al., 2023) and then further decline of dMn along with dCo implicating the dominance of scavenging of dCo by Mn oxidation below oxycline depth (Figure 9, 10a).

In contrast to the Arabian Sea, the BoB shows a scavenging type of profile. This could have a combination of factors such as the low productivity and corresponding lower uptake, combined with high input of dCo from rivers and dust, the presence of Fe-Mn oxyhydroxides and similar scavenging pathway of Mn and Co in the water column, and deeper remineralization of dCo with PO_4^{3-} due to the ballast effect. The surface water exhibits the highest dCo concentration of ~ 0.11 nM which decreases gradually with depth and without any correlation with the nitrite peaks in the water column (Figure 9, 10b). The elevated surface concentration may be attributed to the riverine input as well as atmospheric and shelf supply that aligns with the previous study conducted in the Arctic Ocean (Bundy et al., 2020). Also, waters near the river mouth contain a high concentration of organic ligands that prevents dCo scavenging via Mn oxides (Beck et al., 1974; Lenstra et al., 2022; Shiller et al., 2006) and further transport of these high dCo waters could have raised the surface dCo in BoB. Another contrasting feature is the inverse correlation of dCo with phosphate in the BoB (top 250 m) suggesting the dominance of scavenging over the bio-uptake which is also confirmed by the surface decoupling of the pCo and pP (Weisend, 2017). Hence the peak formed due to remineralisation, like the Arabian Sea and other world oceans in the euphotic zone (oxycline), is not observed in BoB. Rather, a slight increase in the dCo along with phosphate in the deeper OMZ (below 250 m) suggests a deeper remineralisation in the BoB probably due to the ballast effect (Kwon et al., 2009; Rixen et al., 2019). Although the dCo, nitrite, and dMn in the OMZ of the Arabian Sea are well correlated but not in the BoB (Figure 10a and b). Unlike the Arabian Sea, the existence of certain bacterial populations, the anammox process in the water column, and the presence of extremely low DO conditions aided by inhibition of vertical DO supply by strong salinity stratification may account for the nitrite peaks associated with the Bay of Bengal (Bristow et al., 2017). The Co (II) oxidation is associated with a common catalytic site with Mn (II), rather than the non-biologically freshly formed Mn-oxyhydroxides

(Moffett & Ho, 1996) indicating the coupling of Co and Mn is due to the presence of Mn-oxidizing bacteria rather than the abundance of Mn oxides. Further study confirms the oxidation of cobalt via microbial pathways like Mn oxidation as well as via indirect oxidation of the Mn oxides (Murray et al., 2007). The pCo and pMn studies (Weisend, 2017) show a similar scavenging process of Mn and Co via bacterial oxidation in the water column. The peaks of nitrite observed for this region could be due to the supply of organic matter and nitrite by the cross-shelf transport (Udaya Bhaskar et al., 2021). The dCo enrichment in the shelf region could be from the enriched pore waters in shelf sediments. The presence of high suspended particulate matter can be confirmed by the beam attenuation coefficient data obtained from Seabird sensors (see Figure S11).

In the present study, the absence of any nitrite peak near the bottom waters of the shelf region (station GI09/01) indicates the lack of cross-shelf transport of nitrite. This supports water column denitrification in the Oxygen Minimum Zone (OMZ) of the Bay of Bengal (BoB). The Cobalt (Co) gets dissolved from the shelf sediments under anoxic conditions and is released to the bottom waters of the shelf region, (see Figure 9a, depth > 120m). However, the dissolution rate and its further transport is much less compared to Manganese (Mn) and Iron (Fe), implying the absence of any discernible dCo peak corresponding to nitrite peak in the OMZ of central BoB (GI09/02). Previous studies in the Benguela upwelling zone also confirm a much lower flux of dCo compared to dissolved Iron (dFe) and dissolved Manganese (dMn) from the reducing sediments (Liu et al., 2022). Further observations along the Congo River Margin (Vieira et al., 2020) and Peruvian Shelf (Sanial et al., 2018) support such lower release, possibly due to the minimal increase of dCo in suboxic waters (<10 μ M; Liu et al., 2022). The minimal shelf release and transport combined with the significantly large surface concentration of dCo in the northern BoB supplied from external sources such as rivers, SGD and atmospheric sources, makes it challenging to detect any substantial dCo peak coinciding with nitrite peak in the OMZ of northern BoB. However, the modest increase in dCo in low oxygen conditions (below 250 m) is a result of the strong association of dCo with PO₄³⁻ similar to the dissolved Cadmium (dCd) (Ikhsani et al., 2023) due to the ballast effect and deeper remineralization of sinking organic matter (Kwon et al., 2009; Rixen et al., 2019). The input of lithogenic matter to the water column in river-dominated regions of the Indian Ocean has increased the organic carbon flux rate by 62% (Rixen et al., 2019), thereby affecting the remineralization scale length in the BoB water column. All the afore-mentioned discussed factors influence the biogeochemical cycling of dCo in the BoB waters, creating a noticeable difference from the Arabian Sea and other global OMZ regions.

5.6 Impact of global warming on the dCo inventory of the northern Indian Ocean

A few available studies suggest a decreasing trend of DO in the global ocean during recent years resulting in the intensification and expansion of global OMZ (Huang et al., 2023; Stramma et al., 2008). The increase in sea surface temperature due to global warming increases ocean deoxygenation (Keeling et al., 2010) which in turn modifies the extent and intensity of global OMZ including the BoB and the Arabian Sea (Behrenfeld et al., 2006; Falkowski et al., 2011; Ito et al., 2017). The impending variation in the redox condition of the water column due to global warming might influence the biogeochemical cycling of cobalt in the BoB and Arabian Sea releasing more cobalt to the water column due to its reductive dissolution. A rough estimate of dCo increase in the northern Indian Ocean is made based on the rate of change of DO in the Indian Ocean due to global warming. The BoB has a dCo:DO slope of $0.0001 \text{ nM } \mu\text{M}^{-1}$ (Supplementary Figure S10) in the OMZ waters (between 100-1500 m). Considering a decreasing rate of $0.59 \text{ mmol oxygen m}^{-3} \text{ decade}^{-1}$ (Huang et al., 2023), dCo may further increase at a rate of $0.06 \text{ pmol L}^{-1} \text{ decade}^{-1}$ in the BoB. Similarly, the dCo:DO in the OMZ waters of Arabian Sea is observed to be $0.0016 \text{ nM } \mu\text{M}^{-1}$. Hence, with a reported decreasing rate of $1.9 \text{ mmol oxygen m}^{-3} \text{ decade}^{-1}$ (Huang et al., 2023), the dCo will increase at a rate of $3.04 \text{ pmol L}^{-1} \text{ decade}^{-1}$ in the OMZ of the Arabian Sea. These estimates suggest that a total decrease of 0.81 Tmol in DO reservoir in the OMZ of the Bay of Bengal due to global warming will lead to a 0.082 Mmol increase in dCo reservoir in a decade. Similarly, in Arabian Sea, 5.16 Tmol decrease per decade of DO will result in 8.26 Mmol increase of dCo. These estimates were made based on the current inventory of DO and dCo in the OMZ of the BoB and the Arabian Sea and their rates of change of DO per decade. The present study estimates 1.4% decrease in DO will lead to an increase of 0.1% dCo inventory of BoB. Correspondingly, a 19% decrease in DO will lead to a 3.26% increase in the dCo reservoir of Arabian Sea in the coming decade. Such discussions clearly imply that the future global warming will lead to intensification of the OMZ in the Indian Ocean resulting in the increase in dCo inventory of the sea water.

6. Conclusion

The present study illustrates the dCo distribution over the Indian Ocean comprising the BoB, the Arabian Sea, the CIOB, and the SIO (up to 30°S). The dCo has a considerable variation of 0.002 to 0.13 nmol/L in the Indian Ocean. The coastal Arabian Sea has a surface dCo concentration of 0.12-0.13 nmol/L owing to the proximity of the sources from the continents which decreases to 0.02-0.03 nmol/L in the central part. In contrast, the BoB has a higher dCo surface concentration of 0.11 nmol/L not restricting to the coastal part but spreading over the northern BoB that progressively decreases to 0.03 nmol/L in the southern part (5°N). This could be attributed to the combined effect of high riverine

input along with the atmospheric dust, shelf supply, and SGD. In addition, the scavenging type of profile of dCo in the BoB could be linked to low biological productivity and subsequently lower utilisation through biological uptake. The variation in the Co:P slopes (18 to 41 $\mu\text{M M}^{-1}$) progressively increase from the SIO to the Northern Indian Ocean (Arabian Sea) and the intercepts over the different regions of the Indian Ocean are associated with the increased primary productivity along with the community shift.

In the OMZ area of the Arabian Sea, the surface dCo is low (0.037-0.05 nmol/L) due to the biological uptake which increases to 0.115 nmol/L at the oxycline depth associated with the nitrite maxima and dMn peak. However, the OMZ area of the BoB shows a contrasting feature with a scavenging-type surface profile and no pronounced peak at the nitrite maxima. Rather a minor increase in the dCo in the OMZ waters of BoB corresponds to remineralisation of PO_4^{3-} . The above-mentioned contrasting feature between the Arabian Sea and the BoB is due to the different processes associated with them. The peak of dCo in the Arabian Sea OMZ along with nitrite and dMn corresponds to the release of dCo along with dMn associated with the bacterial mediated oxidation. However, in the BoB, the absence of dCo peak with nitrite maxima demonstrates the dominance of scavenging over the bio uptake and remineralisation at deeper depth due to the ballast effect. The deeper water dCo contribution is attributed to the reductive dissolution of the bottom sediments in the coastal BoB (0.060 nmol/L) and the interaction of the subducting polymetallic nodule rich (Fe-Mn, Cu, Ni, Co) oceanic crust with the fluids along the Java-Sumatra subduction Zone (0.05-0.065 nmol/L). The present study reveals intricate biogeochemical cycling processes of dCo in the Indian Ocean and also the difference in dCo cycling between the OMZ of the Arabian Sea and the Bay of Bengal and its link to the future global climate changes.

Open Research

The dCo data, used in the present study have been provided in the Supplementary Information and will also be archived at the institutional (CSIR- National Institute of Oceanography, Goa) data repository centre at the URL, <https://publication-data.nio.res.in/s/jdF5dKXT0a9j7DZ>. The dCo data used for the comparison and validation of sampling and analytical techniques is from Vu and Sohrin (2013). The estimation of Atmospheric flux includes the Al flux data from Xu and Weber (2021). River and groundwater dCo data taken from Samanta and Dalai, (2018), Mishra and Kumar (2020), Akshitha et al (2022). The DO decrease rate and reservoir values were taken from Huang et al. (2023). The spatial maps for soluble Co flux and other section plots are created using ODV software (Version 5.6.3, 2022) (<https://odv.awi.de>, 2022).

Acknowledgments

We express our gratitude to the captain, crew members, chief scientists, and all participants involved in GI09, and GI10 for their valuable support during the collection of samples and the subsequent on-board analysis. All of these endeavors have been undertaken within the framework of the GEOTRACES India initiative. We express our sincere thanks to the Government of India, specifically the Council of Scientific and Industrial Research (CSIR) and the Ministry of Earth Sciences (MoES), for their generous financial support. We additionally convey gratitude to the CSIR-National Institute of Oceanography in Goa, India, and the Physical Research Laboratory in Ahmedabad, India, for their logistic assistance.

References

- Akshitha, V., Balakrishna, K., Hegde, P., & Udayashankar, H. N. (2022). Evaluation of heavy metal contamination and human health risk using geo-statistical techniques in selected shallow hard rock aquifers of southwest India. *Groundwater for Sustainable Development*, 19, 100812. <https://doi.org/10.1016/j.gsd.2022.100812>
- Aswini, M. A., Kumar, A., & Das, S. K. (2020). Quantification of long-range transported aeolian dust towards the Indian peninsular region using satellite and ground-based data - A case study during a dust storm over the Arabian Sea. *Atmospheric Research*, 239, 104910. <https://doi.org/10.1016/j.atmosres.2020.104910>
- Basu, A. R., Jacobsen, S. B., Poreda, R. J., Dowling, C. B., & Aggarwal, P. K. (2001). Large groundwater strontium flux to the oceans from the Bengal Basin and the marine strontium isotope record. *Science (New York, N.Y.)*, 293(5534), 1470–1473. <https://doi.org/10.1126/science.1060524>
- Beck, K. C., Reuter, J. H., & Perdue, E. M. (1974). Organic and inorganic geochemistry of some coastal plain rivers of the southeastern United States. *Geochimica et Cosmochimica Acta*, 38(3), 341–364. [https://doi.org/10.1016/0016-7037\(74\)90130-6](https://doi.org/10.1016/0016-7037(74)90130-6)
- Behrenfeld, M. J., O'Malley, R. T., Siegel, D. A., McClain, C. R., Sarmiento, J. L., Feldman, G. C., et al. (2006). Climate-driven trends in contemporary ocean productivity. *Nature*, 444(7120), 752–755. <https://doi.org/10.1038/nature05317>
- Bikkina, S., Shukla, A., Singh, S. K., Karri, D., Singh, N. D., & Sahoo, B. (2023). Link of the short-term temporal trends of Sr and Nd isotopic composition of aeolian dust over the Arabian Sea with the source emissions. *Science of The Total Environment*, 892, 164680. <https://doi.org/10.1016/j.scitotenv.2023.164680>
- Bown, J., Boye, M., & Nelson, D. M. (2012). New insights on the role of organic speciation in the biogeochemical cycle of dissolved cobalt in the southeastern Atlantic and the Southern Ocean. *Biogeosciences*, 9(7), 2719–2736. <https://doi.org/10.5194/bg-9-2719-2012>
- Bown, Johann, Boye, M., Baker, A., Duviolbourg, E., Lacan, F., Le Moigne, F., et al. (2011). The biogeochemical cycle of dissolved cobalt in the Atlantic and the Southern Ocean south off the coast of South Africa. *Marine Chemistry*, 126, 193–206. <https://doi.org/10.1016/j.marchem.2011.03.008>

- Bristow, L. A., Callbeck, C. M., Larsen, M., Altabet, M. A., Dekaezemacker, J., Forth, M., et al. (2017). N₂ production rates limited by nitrite availability in the Bay of Bengal oxygen minimum zone. *Nature Geoscience*, *10*(1), 24–29. <https://doi.org/10.1038/ngeo2847>
- Bruce, J. G., Kindle, J. C., Kantha, L. H., Kerling, J. L., & Bailey, J. F. (1998). Recent observations and modeling in the Arabian Sea Laccadive High region. *Journal of Geophysical Research: Oceans*, *103*(C4), 7593–7600. <https://doi.org/10.1029/97JC03219>
- Bundy, R. M., Tagliabue, A., Hawco, N. J., Morton, P. L., Twining, B. S., Hatta, M., et al. (2020). Elevated sources of cobalt in the Arctic Ocean. *Biogeosciences*, *17*(19), 4745–4767. <https://doi.org/10.5194/bg-17-4745-2020>
- Carritt, D., & Carpenter, J. (1966). Comparison and evaluation of currently employed modifications of the Winkler method for determining dissolved oxygen in seawater; A NASCO report. *Journal of Marine Research*, *24*(3). Retrieved from https://elischolar.library.yale.edu/journal_of_marine_research/1077
- Chester, R., Berry, A. S., & Murphy, K. J. T. (1991). The distributions of particulate atmospheric trace metals and mineral aerosols over the Indian Ocean. *Marine Chemistry*, *34*(3), 261–290. [https://doi.org/10.1016/0304-4203\(91\)90007-J](https://doi.org/10.1016/0304-4203(91)90007-J)
- Chinni, V., Singh, S. K., Bhushan, R., Rengarajan, R., & Sarma, V. V. S. S. (2018). Spatial variability in dissolved iron concentrations in the marginal and open waters of the Indian Ocean. *Marine Chemistry*, *208*, 11–28. <https://doi.org/10.1016/j.marchem.2018.11.007>
- Chmiel, R., Lanning, N., Laubach, A., Lee, J.-M., Fitzsimmons, J., Hatta, M., et al. (2022). Major processes of the dissolved cobalt cycle in the North and equatorial Pacific Ocean. *Biogeosciences*, *19*(9), 2365–2395. <https://doi.org/10.5194/bg-19-2365-2022>
- Clemens, S. C., Kuhnt, W., LeVay, L. J., & Expedition 353 Scientists. (2016). *Volume 353: Indian Monsoon Rainfall* (Vol. 353). International Ocean Discovery Program. <https://doi.org/10.14379/iodp.proc.353.2016>
- Cowen, J. P., & Bruland, K. W. (1985). Metal deposits associated with bacteria: implications for Fe and Mn marine biogeochemistry. *Deep Sea Research Part A. Oceanographic Research Papers*, *32*(3), 253–272. [https://doi.org/10.1016/0198-0149\(85\)90078-0](https://doi.org/10.1016/0198-0149(85)90078-0)
- Cutter, G., Andersson, P., Codispoti, L., Croot, P., François, R., Lohan, M. C., et al. (2010). Sampling and Sample-handling Protocols for GEOTRACES Cruises [Other]. Retrieved May 27, 2024, from <http://www.geotraces.org/libraries/documents/Intercalibration/Cookbook.pdf>
- Damodararao, K., & Singh, S. K. (2022). Substantial submarine groundwater discharge in the estuaries of the east coast of India and its impact on marine strontium budget. *Geochimica et Cosmochimica Acta*, *324*, 66–85. <https://doi.org/10.1016/j.gca.2022.03.002>
- Dileep Kumar, M., & Li, Y.-H. (1996). Spreading of water masses and regeneration of silica and ²²⁶Ra in the Indian Ocean. *Deep Sea Research Part II: Topical Studies in Oceanography*, *43*(1), 83–110. [https://doi.org/10.1016/0967-0645\(95\)00084-4](https://doi.org/10.1016/0967-0645(95)00084-4)
- Dulaquais, G., Boye, M., Rijkenberg, M. J. A., & Carton, X. (2014). Physical and remineralization processes govern the cobalt distribution in the deep western Atlantic Ocean. *Biogeosciences*, *11*(6), 1561–1580. <https://doi.org/10.5194/bg-11-1561-2014>

- Dulaquais, Gabriel, Planquette, H., L'Helguen, S., Rijkenberg, M. J. A., & Boye, M. (2017). The biogeochemistry of cobalt in the Mediterranean Sea. *Global Biogeochemical Cycles*, *31*(2), 377–399. <https://doi.org/10.1002/2016GB005478>
- Ellwood, M. J. (2008). Wintertime trace metal (Zn, Cu, Ni, Cd, Pb and Co) and nutrient distributions in the Subantarctic Zone between 40–52°S; 155–160°E. *Marine Chemistry*, *112*(1), 107–117. <https://doi.org/10.1016/j.marchem.2008.07.008>
- Falkowski, P. G., Algeo, T., Codispoti, L., Deutsch, C., Emerson, S., Hales, B., et al. (2011). Ocean deoxygenation: Past, present, and future. *Eos, Transactions American Geophysical Union*, *92*(46), 409–410. <https://doi.org/10.1029/2011EO460001>
- Frank, M., Whiteley, N., van de Flierdt, T., Reynolds, B. C., & O'Nions, K. (2006). Nd and Pb isotope evolution of deep water masses in the eastern Indian Ocean during the past 33 Myr. *Chemical Geology*, *226*(3), 264–279. <https://doi.org/10.1016/j.chemgeo.2005.09.024>
- Galy, A., & France-Lanord, C. (2001). Higher erosion rates in the Himalaya: Geochemical constraints on riverine fluxes. *Geology*, *29*(1), 23–26. [https://doi.org/10.1130/0091-7613\(2001\)029<0023:HERITH>2.0.CO;2](https://doi.org/10.1130/0091-7613(2001)029<0023:HERITH>2.0.CO;2)
- Garrison, D. L., Gowing, M. M., Hughes, M. P., Campbell, L., Caron, D. A., Dennett, M. R., et al. (2000). Microbial food web structure in the Arabian Sea: a US JGOFS study. *Deep Sea Research Part II: Topical Studies in Oceanography*, *47*(7), 1387–1422. [https://doi.org/10.1016/S0967-0645\(99\)00148-4](https://doi.org/10.1016/S0967-0645(99)00148-4)
- Goswami, V., Singh, S. K., & Bhushan, R. (2014). Impact of water mass mixing and dust deposition on Nd concentration and ϵNd of the Arabian Sea water column. *Geochimica et Cosmochimica Acta*, *145*, 30–49. <https://doi.org/10.1016/j.gca.2014.09.006>
- Gupta, H., Reddy, K. K., Gandla, V., Paridula, L., Chiluka, M., & Vashisth, B. (2022). Freshwater discharge from the large and coastal peninsular rivers of India: A reassessment for sustainable water management. *Environmental Science and Pollution Research*, *29*(10), 14400–14417. <https://doi.org/10.1007/s11356-021-16811-0>
- Hawco, N., Lam, P. J., Lee, J. M., Ohnemus, D. C., Noble, A. E., Wyatt, N., et al. (2018). Cobalt scavenging in the mesopelagic ocean and its influence on global mass balance: Synthesizing water column and sedimentary fluxes. *Marine Chemistry*, *201*, 151–166. <https://doi.org/10.1016/j.marchem.2017.09.001>
- Hawco, N. J., & Saito, M. A. (2018). Competitive inhibition of cobalt uptake by zinc and manganese in a pacific *Prochlorococcus* strain: Insights into metal homeostasis in a streamlined oligotrophic cyanobacterium. *Limnology and Oceanography*, *63*(5), 2229–2249. <https://doi.org/10.1002/lno.10935>
- Hawco, N. J., Ohnemus, D. C., Resing, J. A., Twining, B. S., & Saito, M. A. (2016). A dissolved cobalt plume in the oxygen minimum zone of the eastern tropical South Pacific. *Biogeosciences*, *13*(20), 5697–5717. <https://doi.org/10.5194/bg-13-5697-2016>
- Huang, S., Shao, J., Chen, Y., Qi, J., Wu, S., Zhang, F., et al. (2023). Reconstruction of dissolved oxygen in the Indian Ocean from 1980 to 2019 based on machine learning techniques. *Frontiers in Marine Science*, *10*. <https://doi.org/10.3389/fmars.2023.1291232>

- Ikhsani, I. Y., Wong, K. H., Ogawa, H., & Obata, H. (2023). Dissolved trace metals (Fe, Mn, Pb, Cd, Cu, and Zn) in the eastern Indian Ocean. *Marine Chemistry*, 248, 104208. <https://doi.org/10.1016/j.marchem.2023.104208>
- Ito, T., Minobe, S., Long, M. C., & Deutsch, C. (2017). Upper ocean O₂ trends: 1958–2015. *Geophysical Research Letters*, 44(9), 4214–4223. <https://doi.org/10.1002/2017GL073613>
- Ittekkot, V., & Haake, B. (1990). The terrestrial link in the removal of organic carbon in the sea. *Facets of Modern Biogeochemistry*, 318.
- Karri, D., Bikkina, S., & Singh, S. K. (2024). Tracing the provenance of mineral dust over the northern and southern Indian Oceans during the GEOTRACES-India (GI-01, GI-02) expeditions. *Geochimica et Cosmochimica Acta*, 366, 141–153. <https://doi.org/10.1016/j.gca.2023.12.025>
- Keeling, R. F., Körtzinger, A., & Gruber, N. (2010). Ocean Deoxygenation in a Warming World. *Annual Review of Marine Science*, 2(1), 199–229. <https://doi.org/10.1146/annurev.marine.010908.163855>
- Kharkar, D. P., Turekian, K. K., & Bertine, K. K. (1968). Stream supply of dissolved silver, molybdenum, antimony, selenium, chromium, cobalt, rubidium and cesium to the oceans. *Geochimica et Cosmochimica Acta*, 32(3), 285–298. [https://doi.org/10.1016/0016-7037\(68\)90016-1](https://doi.org/10.1016/0016-7037(68)90016-1)
- Kumar, A., Sudheer, A. K., Goswami, V., & Bhushan, R. (2012). Influence of continental outflow on aerosol chemical characteristics over the Arabian Sea during winter. *Atmospheric Environment*, 50, 182–191. <https://doi.org/10.1016/j.atmosenv.2011.12.040>
- Kumar, A., Suresh, K., & Rahaman, W. (2020). Geochemical characterization of modern aeolian dust over the Northeastern Arabian Sea: Implication for dust transport in the Arabian Sea. *Science of the Total Environment*, 729. <https://doi.org/10.1016/j.scitotenv.2020.138576>
- Kwon, E. Y., Primeau, F., & Sarmiento, J. L. (2009). The impact of remineralization depth on the air–sea carbon balance. *Nature Geoscience*, 2(9), 630–635. <https://doi.org/10.1038/ngeo612>
- Lane, T. W., & Morel, F. M. M. (2000). Regulation of Carbonic Anhydrase Expression by Zinc, Cobalt, and Carbon Dioxide in the Marine Diatom *Thalassiosira weissflogii* 1. *Plant Physiology*, 123(1), 345–352. <https://doi.org/10.1104/pp.123.1.345>
- Laxman, M. B., Nagaraju, B., Nagaraju, K., & Kumar, K. V. (2022). Spatial variations in the geochemical characteristics of basalts from the Deccan Volcanic Province, India: Role of mixing and assimilation fractional crystallisation. *Journal of Earth System Science*, 131(3), 186. <https://doi.org/10.1007/s12040-022-01922-0>
- Lenstra, W. K., van Helmond, N. A. G. M., Żygadłowska, O. M., van Zummeren, R., Witbaard, R., & Slomp, C. P. (2022). Sediments as a Source of Iron, Manganese, Cobalt and Nickel to Continental Shelf Waters (Louisiana, Gulf of Mexico). *Frontiers in Marine Science*, 9. Retrieved from <https://www.frontiersin.org/articles/10.3389/fmars.2022.811953>
- Lino, Y., Udayashankar, H. N., Suresh Babu, D. S., Ramasamy, M., & Balakrishna, K. (2023). Large submarine groundwater discharges to the Arabian Sea from tropical southwestern Indian Coast: Measurements from seepage meters deployed during the low tide. *Journal of Hydrology*, 620, 129394. <https://doi.org/10.1016/j.jhydrol.2023.129394>

- Liu, T., Krisch, S., Xie, R. C., Hopwood, M. J., Dengler, M., & Achterberg, E. P. (2022). Sediment Release in the Benguela Upwelling System Dominates Trace Metal Input to the Shelf and Eastern South Atlantic Ocean. *Global Biogeochemical Cycles*, 36(9). <https://doi.org/10.1029/2022gb007466>
- Whitfield, M. & Turner, D.R.. (1987). The role of particles in regulating the composition of seawater. *Aquatic Surface Chemistry*, 457–493.
- Madhupratap, M., Gauns, M., Ramaiah, N., Prasanna Kumar, S., Muraleedharan, P. M., de Sousa, S. N., et al. (2003). Biogeochemistry of the Bay of Bengal: physical, chemical and primary productivity characteristics of the central and western Bay of Bengal during summer monsoon 2001. *Deep Sea Research Part II: Topical Studies in Oceanography*, 50(5), 881–896. [https://doi.org/10.1016/S0967-0645\(02\)00611-2](https://doi.org/10.1016/S0967-0645(02)00611-2)
- Mantyla, A. W., & Reid, J. L. (1995). On the origins of deep and bottom waters of the Indian Ocean. *Journal of Geophysical Research: Oceans*, 100(C2), 2417–2439. <https://doi.org/10.1029/94JC02564>
- Matondkar, S. G. P., Parab, S. G., Desa, E., & Dwivedi, R. M. (2006). Basin scale distribution of Trichodesmium spp. in the Arabian Sea using Oceansat I/OCM. In *Remote Sensing of the Marine Environment* (Vol. 6406, pp. 226–235). SPIE. <https://doi.org/10.1117/12.693687>
- Milliman, J. D., & Meade, R. H. (1983). World-Wide Delivery of River Sediment to the Oceans. *The Journal of Geology*, 1. <https://doi.org/10.1086/628741>
- Miriyala, P., Sukumaran, N. P., Nath, B. N., Ramamurty, P. B., Sijinkumar, A. V., Vijayagopal, B., et al. (2017). Increased chemical weathering during the deglacial to mid-Holocene summer monsoon intensification. *Scientific Reports*, 7(October 2016), 1–11. <https://doi.org/10.1038/srep44310>
- Mishra, S., & Kumar, D. (2020). Estimation of physicochemical characteristics and associated metal contamination risk in river Narmada, India. *Environmental Engineering Research*, 26. <https://doi.org/10.4491/eer.2019.521>
- Moffett, J. W., & Ho, J. (1996). Oxidation of cobalt and manganese in seawater via a common microbially catalyzed pathway. *Geochimica et Cosmochimica Acta*, 60(18), 3415–3424. [https://doi.org/10.1016/0016-7037\(96\)00176-7](https://doi.org/10.1016/0016-7037(96)00176-7)
- Morel, F. M. M., & Price, N. M. (2003). The biogeochemical cycles of trace metals in the oceans. *Science*, 300(5621), 944–947. <https://doi.org/10.1126/science.1083545>
- Murray, K. J., Webb, S. M., Bargar, J. R., & Tebo, B. M. (2007). Indirect Oxidation of Co(II) in the Presence of the Marine Mn(II)-Oxidizing Bacterium Bacillus sp. Strain SG-1. *Applied and Environmental Microbiology*, 73(21), 6905–6909. <https://doi.org/10.1128/AEM.00971-07>
- Murty, V. s. N., Y.V.B, S., Rao, D. P., & Murty, C. S. (1992). Water characteristics, mixing and circulation in the Bay of Bengal during southwest monsoon. *Journal of Marine Research*, 50. <https://doi.org/10.1357/002224092784797700>
- Nishioka, J., Obata, H., & Tsumune, D. (2013). Evidence of an extensive spread of hydrothermal dissolved iron in the Indian Ocean. *Earth and Planetary Science Letters*, 361, 26–33. <https://doi.org/10.1016/j.epsl.2012.11.040>
- Noble, A. E., Saito, M. A., Maiti, K., & Benitez-Nelson, C. R. (2008). Cobalt, manganese, and iron near the Hawaiian Islands: A potential concentrating mechanism for cobalt within a cyclonic eddy and

- implications for the hybrid-type trace metals. *Deep Sea Research Part II: Topical Studies in Oceanography*, 55(10), 1473–1490. <https://doi.org/10.1016/j.dsr2.2008.02.010>
- Noble, A. E., Lamborg, C. H., Ohnemus, D. C., Lam, P. J., Goepfert, T. J., Measures, C. I., et al. (2012). Basin-scale inputs of cobalt, iron, and manganese from the Benguela-Angola front to the South Atlantic Ocean. *Limnology and Oceanography*, 57(4), 989–1010. <https://doi.org/10.4319/lo.2012.57.4.0989>
- Noble, A. E., Ohnemus, D. C., Hawco, N. J., Lam, P. J., & Saito, M. A. (2017). Coastal sources, sinks and strong organic complexation of dissolved cobalt within the US North Atlantic GEOTRACES transect GA03. *Biogeosciences*, 14(11), 2715–2739. <https://doi.org/10.5194/bg-14-2715-2017>
- Nozaki, Y. (1997). A fresh look at element distribution in the North Pacific Ocean. *Eos, Transactions American Geophysical Union*, 78(21), 221–221. <https://doi.org/10.1029/97EO00148>
- Pattan, J. N., Parthiban, G., Amonkar, A., Shaikh, S. A., & Jai Sankar, S. (2017). Trace elements in ferromanganese nodules from the central Indian Ocean basin. *Marine Georesources & Geotechnology*, 35(8), 1147–1157. <https://doi.org/10.1080/1064119X.2017.1297878>
- Prakash, R., Srinivasamoorthy, K., Sundarapandian, S. M., Nanthakumar, C., Gopinath, S., Saravanan, K., & Vinnarasi, F. (2021). Submarine Groundwater Discharge from an Urban Estuary to Southeastern Bay of Bengal, India: Revealed by Trace Element Fluxes. *Archives of Environmental Contamination and Toxicology*, 80(1), 208–233. <https://doi.org/10.1007/s00244-020-00774-3>
- Rahaman, W., & Singh, S. K. (2012). Sr and $^{87}\text{Sr}/^{86}\text{Sr}$ in estuaries of western India: Impact of submarine groundwater discharge. *Geochimica et Cosmochimica Acta*, 85, 275–288. <https://doi.org/10.1016/j.gca.2012.02.025>
- Rao, A. R., Rao, G. N., P. Sreenivas, & Kumar, P. V. H. (2013). Role of Meso-Scale Eddies on Circulation in the South Eastern Arabian Sea in 2009. Retrieved December 6, 2022, from <https://www.tandfonline.com/doi/epdf/10.1080/01490419.2013.811448?needAccess=true&role=button>
- Ray, D., Kamesh Raju, K. A., Baker, E. T., Srinivas Rao, A., Mudholkar, A. V., Lupton, J. E., et al. (2012). Hydrothermal plumes over the Carlsberg Ridge, Indian Ocean. *Geochemistry, Geophysics, Geosystems*, 13(1). <https://doi.org/10.1029/2011GC003888>
- Ray, D., KameshRaju, K. A., Srinivas Rao, A., SuryaPrakash, L., Mudholkar, A. V., Yatheesh, V., et al. (2020). Elevated turbidity and dissolved manganese in deep water column near 10°47'S Central Indian Ridge: studies on hydrothermal activities. *Geo-Marine Letters*, 40(5), 619–628. <https://doi.org/10.1007/s00367-020-00657-5>
- Rixen, T., Gaye, B., Emeis, K.-C., & Ramaswamy, V. (2019). The ballast effect of lithogenic matter and its influences on the carbon fluxes in the Indian Ocean. *Biogeosciences*, 16(2), 485–503. <https://doi.org/10.5194/bg-16-485-2019>
- Robinson, R. a. J., Bird, M. I., Oo, N. W., Hoey, T. B., Aye, M. M., Higgitt, D. L., et al. (2007). The Irrawaddy River Sediment Flux to the Indian Ocean: The Original Nineteenth-Century Data Revisited. *The Journal of Geology*, 115(6), 629–640. <https://doi.org/10.1086/521607>
- Saito, M. A., Goepfert, T. J., Noble, A. E., Bertrand, E. M., Sedwick, P. N., & DiTullio, G. R. (2010). A seasonal study of dissolved cobalt in the Ross Sea, Antarctica: micronutrient behavior, absence of

scavenging, and relationships with Zn, Cd, and P. *Biogeosciences*, 7(12), 4059–4082. <https://doi.org/10.5194/bg-7-4059-2010>

Saito, Mak A., & Moffett, J. W. (2002). Temporal and spatial variability of cobalt in the Atlantic Ocean. *Geochimica et Cosmochimica Acta*, 66(11), 1943–1953. [https://doi.org/10.1016/S0016-7037\(02\)00829-3](https://doi.org/10.1016/S0016-7037(02)00829-3)

Saito, Mak A., Moffett, J. W., Chisholm, S. W., & Waterbury, J. B. (2002). Cobalt limitation and uptake in *Prochlorococcus*. *Limnology and Oceanography*, 47(6), 1629–1636. <https://doi.org/10.4319/lo.2002.47.6.1629>

Saito, Mak A., Moffett, J. W., & DiTullio, G. R. (2004). Cobalt and nickel in the Peru upwelling region: A major flux of labile cobalt utilized as a micronutrient. *Global Biogeochemical Cycles*, 18(4). <https://doi.org/10.1029/2003GB002216>

Saito, Mak A., Rocap, G., & Moffett, J. W. (2005). Production of cobalt binding ligands in a *Synechococcus* feature at the Costa Rica upwelling dome. *Limnology and Oceanography*, 50(1), 279–290. <https://doi.org/10.4319/lo.2005.50.1.0279>

Saito, Mak A., Noble, A. E., Hawco, N., Twining, B. S., Ohnemus, D. C., John, S. G., et al. (2017). The acceleration of dissolved cobalt's ecological stoichiometry due to biological uptake, remineralization, and scavenging in the Atlantic Ocean. *Biogeosciences*, 14(20), 4637–4662. <https://doi.org/10.5194/bg-14-4637-2017>

Samanta, S., & Dalai, T. K. (2018). Massive production of heavy metals in the Ganga (Hooghly) River estuary, India: Global importance of solute-particle interaction and enhanced metal fluxes to the oceans. *Geochimica et Cosmochimica Acta*, 228, 243–258. <https://doi.org/10.1016/j.gca.2018.03.002>

Sanial, V., Kipp, L. E., Henderson, P. B., van Beek, P., Reyss, J.-L., Hammond, D. E., et al. (2018). Radium-228 as a tracer of dissolved trace element inputs from the Peruvian continental margin. *Marine Chemistry*, 201, 20–34. <https://doi.org/10.1016/j.marchem.2017.05.008>

Sarin, M. M., Krishnaswami, S., Dilli, K., Somayajulu, B. L. K., & Moore, W. S. (1989). Major ion chemistry of the Ganga-Brahmaputra river system: Weathering processes and fluxes to the Bay of Bengal. *Geochimica et Cosmochimica Acta*, 53(5), 997–1009. [https://doi.org/10.1016/0016-7037\(89\)90205-6](https://doi.org/10.1016/0016-7037(89)90205-6)

Sarma, V. V. S. S., Rao, G. D., Viswanadham, R., Sherin, C. K., Salisbury, J., Omand, M., et al. (2016). Effects of Freshwater Stratification on Nutrients, Dissolved Oxygen, and Phytoplankton in the Bay of Bengal. *Oceanography*, 29(2), 222–231. <https://doi.org/10.5670/oceanog.2016.54>

Schott, F. A., & McCreary, J. P. (2001). The monsoon circulation of the Indian Ocean. *Progress in Oceanography*, 51(1), 1–123. [https://doi.org/10.1016/S0079-6611\(01\)00083-0](https://doi.org/10.1016/S0079-6611(01)00083-0)

Sengupta, D., Bharath Raj, G. N., & Shenoi, S. S. C. (2006). Surface freshwater from Bay of Bengal runoff and Indonesian Throughflow in the tropical Indian Ocean. *Geophysical Research Letters*, 33(22). <https://doi.org/10.1029/2006GL027573>

Shankar, D., & Shetye, S. R. (1997). On the dynamics of the Lakshadweep high and low in the southeastern Arabian Sea. *Journal of Geophysical Research: Oceans*, 102(C6), 12551–12562. <https://doi.org/10.1029/97JC00465>

- Shelley, R. U., Sedwick, P. N., Bibby, T. S., Cabedo-Sanz, P., Church, T. M., Johnson, R. J., et al. (2012). Controls on dissolved cobalt in surface waters of the Sargasso Sea: Comparisons with iron and aluminum. *Global Biogeochemical Cycles*, 26(2). <https://doi.org/10.1029/2011GB004155>
- Shenoi, S. S. C., Shetye, S. R., Gouveia, A. D., & Michael, G. S. (1993). Salinity extrema in the Arabian Sea. *Monsoon Biogeochemistry*, 76, 37–49.
- Shiller, A. M., Duan, S., van Erp, P., & Bianchi, T. S. (2006). Photo-oxidation of dissolved organic matter in river water and its effect on trace element speciation. *Limnology and Oceanography*, 51(4), 1716–1728. <https://doi.org/10.4319/lo.2006.51.4.1716>
- Singh, N. D., Chinni, V., & Singh, S. K. (2020). Dissolved aluminium cycling in the northern, equatorial and subtropical gyre region of the Indian Ocean. *Geochimica et Cosmochimica Acta*, 268, 160–185. <https://doi.org/10.1016/j.gca.2019.09.028>
- Singh, N. D., Singh, S. K., Malla, N., & Chinni, V. (2023). Biogeochemical cycling of dissolved manganese in the Arabian Sea. *Geochimica et Cosmochimica Acta*, 343, 396–415. <https://doi.org/10.1016/j.gca.2022.12.030>
- Singh, S. K., Rai, S. K., & Krishnaswami, S. (2008). Sr and Nd isotopes in River sediments from the Ganga basin: Sediment provenance and spatial variability in physical erosion. *Journal of Geophysical Research: Earth Surface*, 113(3), 1–18. <https://doi.org/10.1029/2007JF000909>
- Singh, S. P., Singh, S. K., Goswami, V., Bhushan, R., & Rai, V. K. (2012). Spatial distribution of dissolved neodymium and ϵNd in the Bay of Bengal: Role of particulate matter and mixing of water masses. *Geochimica et Cosmochimica Acta*, 94, 38–56. <https://doi.org/10.1016/j.gca.2012.07.017>
- Song, Q., Gordon, A. L., & Visbeck, M. (2004). Spreading of the Indonesian Throughflow in the Indian Ocean. *Journal of Physical Oceanography*, 34(4), 772–792. [https://doi.org/10.1175/1520-0485\(2004\)034<0772:SOTITI>2.0.CO;2](https://doi.org/10.1175/1520-0485(2004)034<0772:SOTITI>2.0.CO;2)
- Srinivas, B., & Sarin, M. M. (2013). Atmospheric dry-deposition of mineral dust and anthropogenic trace metals to the Bay of Bengal. *Journal of Marine Systems*, 126, 56–68. <https://doi.org/10.1016/j.jmarsys.2012.11.004>
- Srinivasan, A., Top, Z., Schlosser, P., Hohmann, R., Iskandarani, M., Olson, D. B., et al. (2004). Mantle ^3He distribution and deep circulation in the Indian Ocean. *Journal of Geophysical Research: Oceans*, 109(C6). <https://doi.org/10.1029/2003JC002028>
- Stramma, L., Johnson, G. C., Sprintall, J., & Mohrholz, V. (2008). Expanding Oxygen-Minimum Zones in the Tropical Oceans. *Science*, 320(5876), 655–658. <https://doi.org/10.1126/science.1153847>
- Suresh, K., Singh, U., Kumar, A., Karri, D., Peketi, A., & Ramaswamy, V. (2021). Provenance tracing of long-range transported dust over the Northeastern Arabian Sea during the southwest monsoon. *Atmospheric Research*, 250, 105377. <https://doi.org/10.1016/j.atmosres.2020.105377>
- Swanner, E. D., Planavsky, N. J., Lalonde, S. V., Robbins, L. J., Bekker, A., Rouxel, O. J., et al. (2014). Cobalt and marine redox evolution. *Earth and Planetary Science Letters*, 390, 253–263. <https://doi.org/10.1016/j.epsl.2014.01.001>

- Tagliabue, A., Hawco, N. J., Bundy, R. M., Landing, W. M., Milne, A., Morton, P. L., & Saito, M. A. (2018). The Role of External Inputs and Internal Cycling in Shaping the Global Ocean Cobalt Distribution: Insights From the First Cobalt Biogeochemical Model. *Global Biogeochemical Cycles*, 32(4), 594–616. <https://doi.org/10.1002/2017GB005830>
- Tindale, N. W., & Pease, P. P. (1999). Aerosols over the Arabian Sea: Atmospheric transport pathways and concentrations of dust and sea salt. *Deep-Sea Research II*, 46, 1577–1595.
- Toole, J. M., & Warren, B. A. (1993). A hydrographic section across the subtropical South Indian Ocean. *Deep Sea Research Part I: Oceanographic Research Papers*, 40(10), 1973–2019. [https://doi.org/10.1016/0967-0637\(93\)90042-2](https://doi.org/10.1016/0967-0637(93)90042-2)
- Udaya Bhaskar, T. V. S., Sarma, V. V. S. S., & Pavan Kumar, J. (2021). Potential Mechanisms Responsible for Spatial Variability in Intensity and Thickness of Oxygen Minimum Zone in the Bay of Bengal. *Journal of Geophysical Research: Biogeosciences*, 126(6), e2021JG006341. <https://doi.org/10.1029/2021JG006341>
- Valsangkar, A. B., Khadge, N. H., & Desa, J. A. E. (1992). Geochemistry of polymetallic nodules from the Central Indian Ocean Basin. *Marine Geology*, 103(1–3), 361–371. [https://doi.org/10.1016/0025-3227\(92\)90026-E](https://doi.org/10.1016/0025-3227(92)90026-E)
- Vieira, L. H., Krisch, S., Hopwood, M. J., Beck, A. J., Scholten, J., Liebetrau, V., & Achterberg, E. P. (2020). Unprecedented Fe delivery from the Congo River margin to the South Atlantic Gyre. *Nature Communications*, 11(1), 556. <https://doi.org/10.1038/s41467-019-14255-2>
- Vu, T. D. H., & Sohrin, Y. (2013). Diverse stoichiometry of dissolved trace metals in the Indian Ocean. *Scientific Reports*, 3. <https://doi.org/10.1038/srep01745>
- Weisend, R. E. (2017). Elemental Ratios of Bioactive Trace Metals in Suspended Particulate Matter in the Bay of Bengal. Retrieved from <https://diginole.lib.fsu.edu/islandora/object/fsu%3A310079/>
- Winkler, L. W. (1888). Die Bestimmung des im Wasser gelösten Sauerstoffes. *Berichte Der Deutschen Chemischen Gesellschaft*, 21(2), 2843–2854. <https://doi.org/10.1002/cber.188802102122>
- Wyrtki, K. (1973). Physical Oceanography of the Indian Ocean. In B. Zeitzschel & S. A. Gerlach (Eds.), *The Biology of the Indian Ocean* (pp. 18–36). Berlin, Heidelberg: Springer. https://doi.org/10.1007/978-3-642-65468-8_3
- Xu, H., & Weber, T. (2021). Ocean Dust Deposition Rates Constrained in a Data-Assimilation Model of the Marine Aluminum Cycle. *Global Biogeochemical Cycles*, 35(9), e2021GB007049. <https://doi.org/10.1029/2021GB007049>
- Yee, D., & Morel, F. M. M. (1996). In vivo substitution of zinc by cobalt in carbonic anhydrase of a marine diatom. *Limnology and Oceanography*, 41(3), 573–577. <https://doi.org/10.4319/lo.1996.41.3.0573>
- Yellappa, T., & Rao, J. M. (2018). Geochemical characteristics of Proterozoic granite magmatism from Southern Granulite Terrain, India: Implications for Gondwana. *Journal of Earth System Science*, 127(2), 22. <https://doi.org/10.1007/s12040-018-0923-6>

You, Y., & Tomczak, M. (1993). Thermocline circulation and ventilation in the Indian Ocean derived from water mass analysis. *Deep Sea Research Part I: Oceanographic Research Papers*, 40(1), 13–56. [https://doi.org/10.1016/0967-0637\(93\)90052-5](https://doi.org/10.1016/0967-0637(93)90052-5)

You, Yuzhu. (1997). Seasonal variations of thermocline circulation and ventilation in the Indian Ocean. *Journal of Geophysical Research: Oceans*, 102(C5), 10391–10422. <https://doi.org/10.1029/96JC03600>

You, Yuzhu. (1998). Intermediate water circulation and ventilation of the Indian Ocean derived from water-mass contributions. *Journal of Marine Research*, 56(5), 1029–1067. <https://doi.org/10.1357/002224098765173455>

You, Yuzhu. (2000). Implications of the deep circulation and ventilation of the Indian Ocean on the renewal mechanism of North Atlantic Deep Water. *Journal of Geophysical Research: Oceans*, 105(C10), 23895–23926. <https://doi.org/10.1029/2000JC900105>

Zhang, H., Van Den Berg, C. M. G., & Wollast, R. (1990). The determination of interactions of cobalt (II) with organic compounds in seawater using cathodic stripping voltammetry. *Marine Chemistry*, 28(4), 285–300. [https://doi.org/10.1016/0304-4203\(90\)90049-I](https://doi.org/10.1016/0304-4203(90)90049-I)

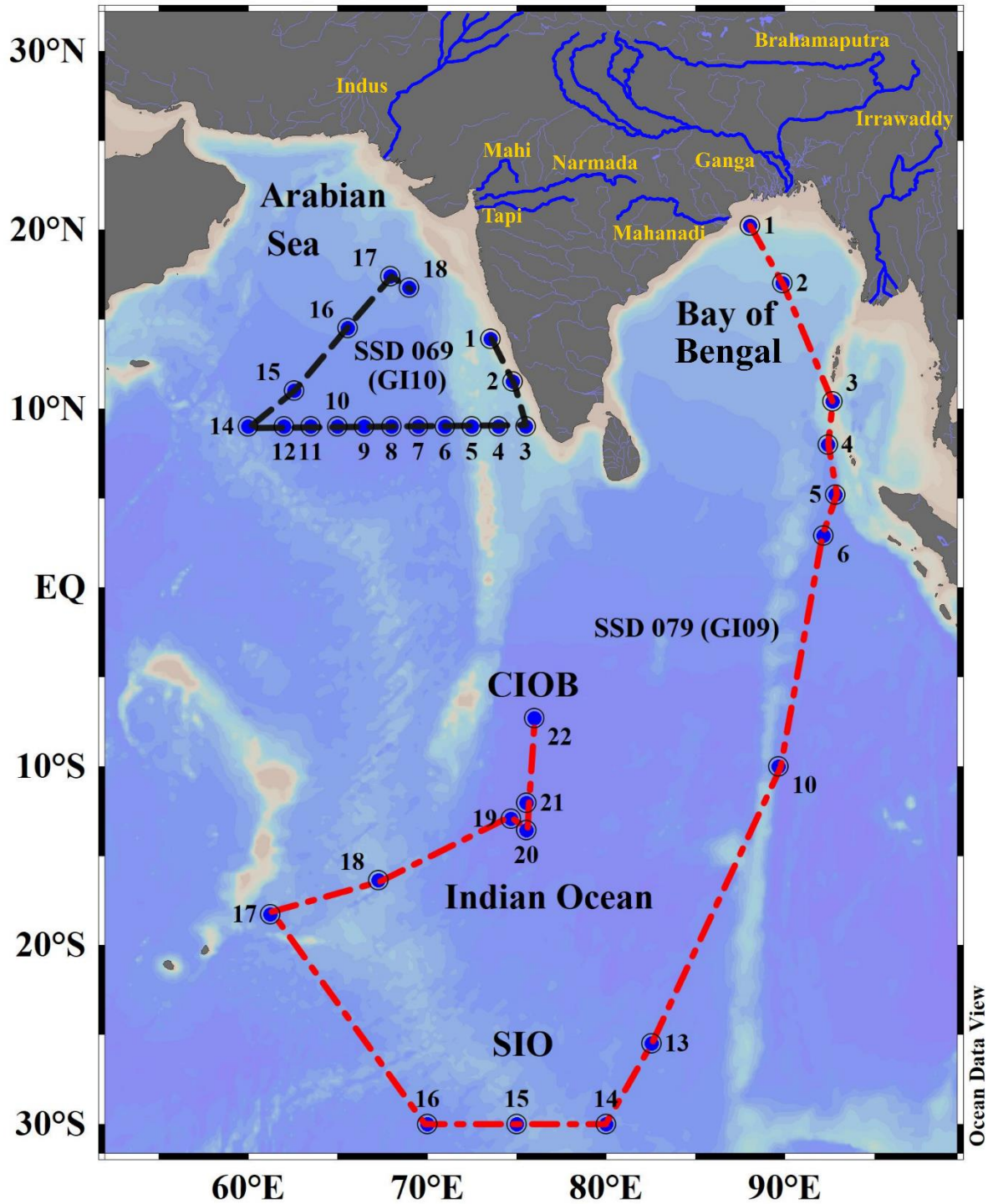


Figure 1: The cruise tracks of GI10 (SSD069) and GI09 (SSD079) and the location of the sampling stations in the Indian Ocean. The GI10 cruise was conducted during January- February 2020 whereas cruise GI09 was completed during March- June 2021. Major rivers flowing to the Bay of Bengal and the Arabian Sea are also shown in the map.

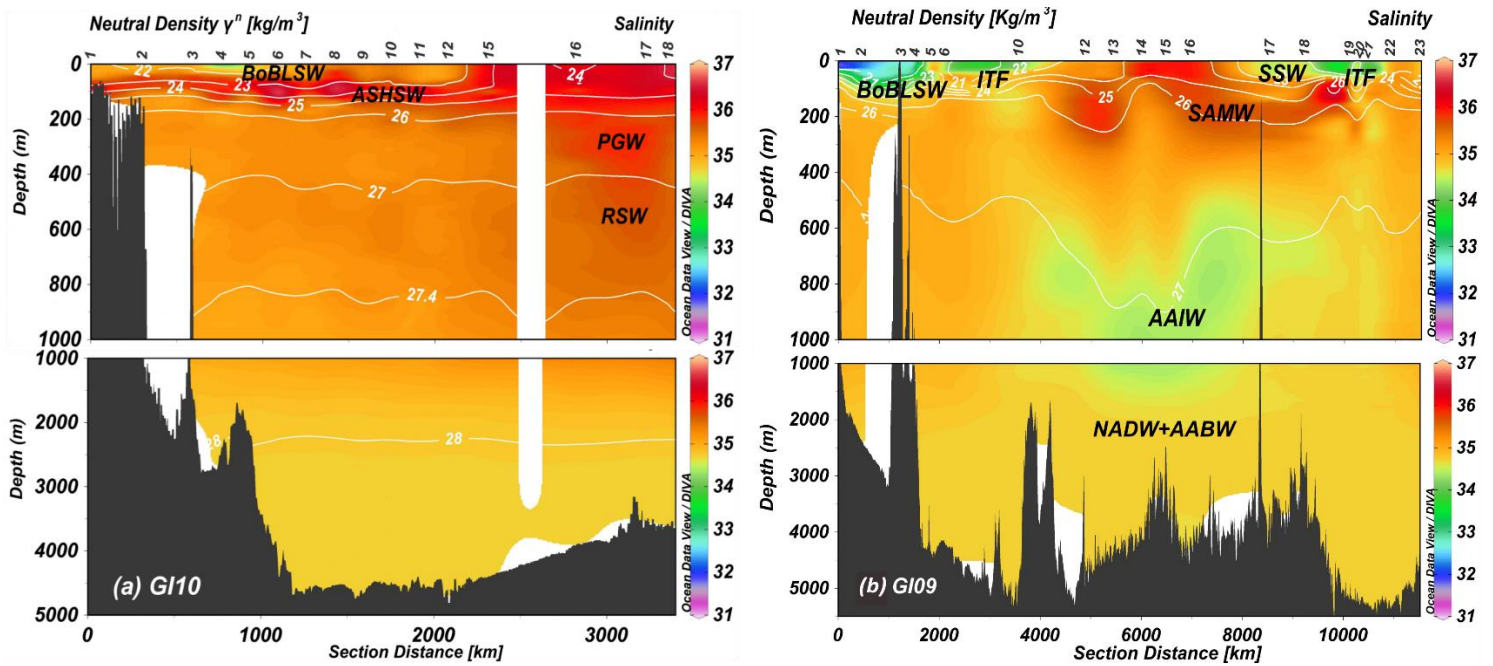


Figure 2: Section plots showing the salinity with the density contours in the Indian Ocean labelled with different water masses, BoBLSW (Bay of Bengal Low Saline water), ASHSW (Arabian Sea High Saline Water), PGW (Persian Gulf Water), RSW (Red Sea Water), ITF (Indonesian Through Flow), SSW (Subtropical Surface Water), SAMW (Subantarctic Mode Water), AAIW (Antarctic Intermediate Water), NADW (North Atlantic Deep Water), AABW (Antarctic Bottom Water) along the cruise tracks of (a) GI10 and (b) GI09.

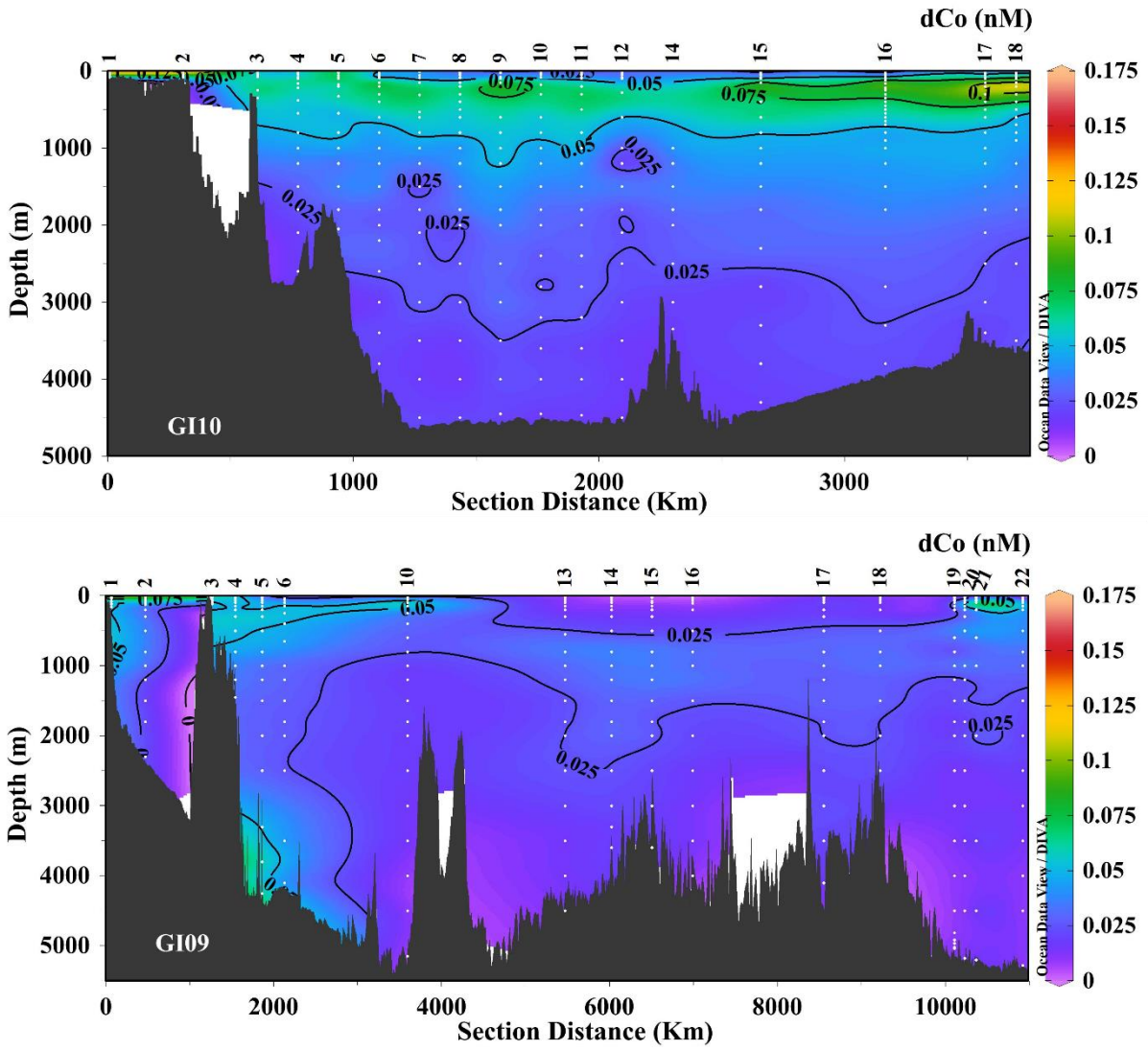


Figure 3: Section plots of dCo along the cruise tracks (a) GI10 in the Arabian Sea, (b) GI09 covering the Bay of Bengal (BoB), Central Indian Ocean Basin (CIOB), and Southern sector of Indian Ocean (SIO). Section plots clearly show the high dCo in the coastal areas, OMZ, and the Subduction Zone deep waters

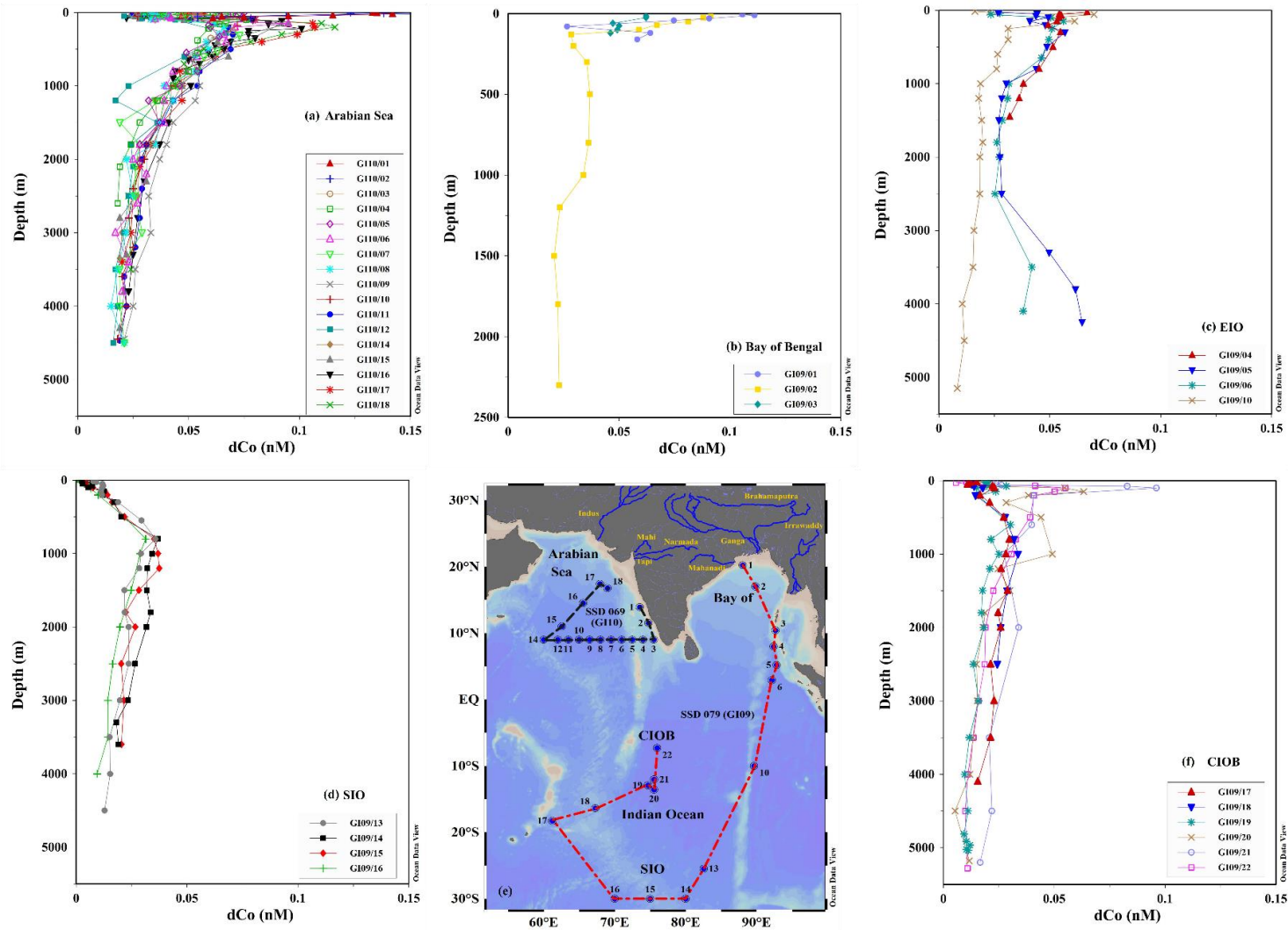


Figure 4: Profiles of dCo in the Indian Ocean along the cruise tracks of GI09 and GI10. Profiles are segregated region wise (a) Arabian Sea, (b) Bay of Bengal, (c) Equatorial Indian Ocean (EIO) (Eastern) (d) Southern sector of Indian Ocean (SIO), (f) Central Indian Ocean Basin (CIOB). (e) Location map of all the stations plotted in this figure. The profiles of different stations are distinguished with different colours and markers mentioned in the legend box of each plot.

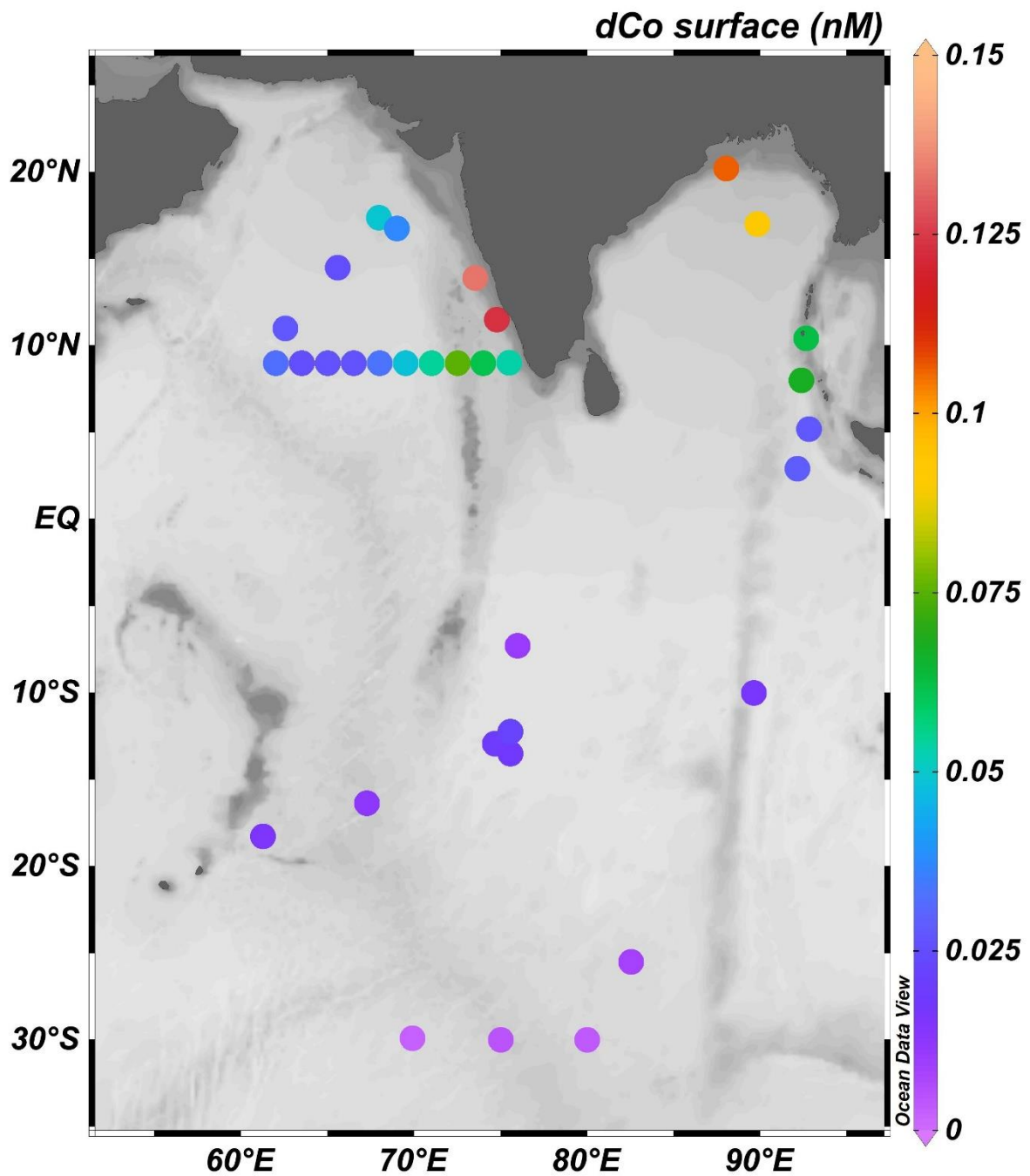


Figure 2: Spatial distribution of the surface dCo (nM) concentration over the Indian Ocean. Higher dCo is observed in the coastal areas of the Northern Indian Ocean (Arabian Sea and Bay of Bengal). The dCo value gradually decreases as we move from the northern to the Southern sector of the Indian Ocean

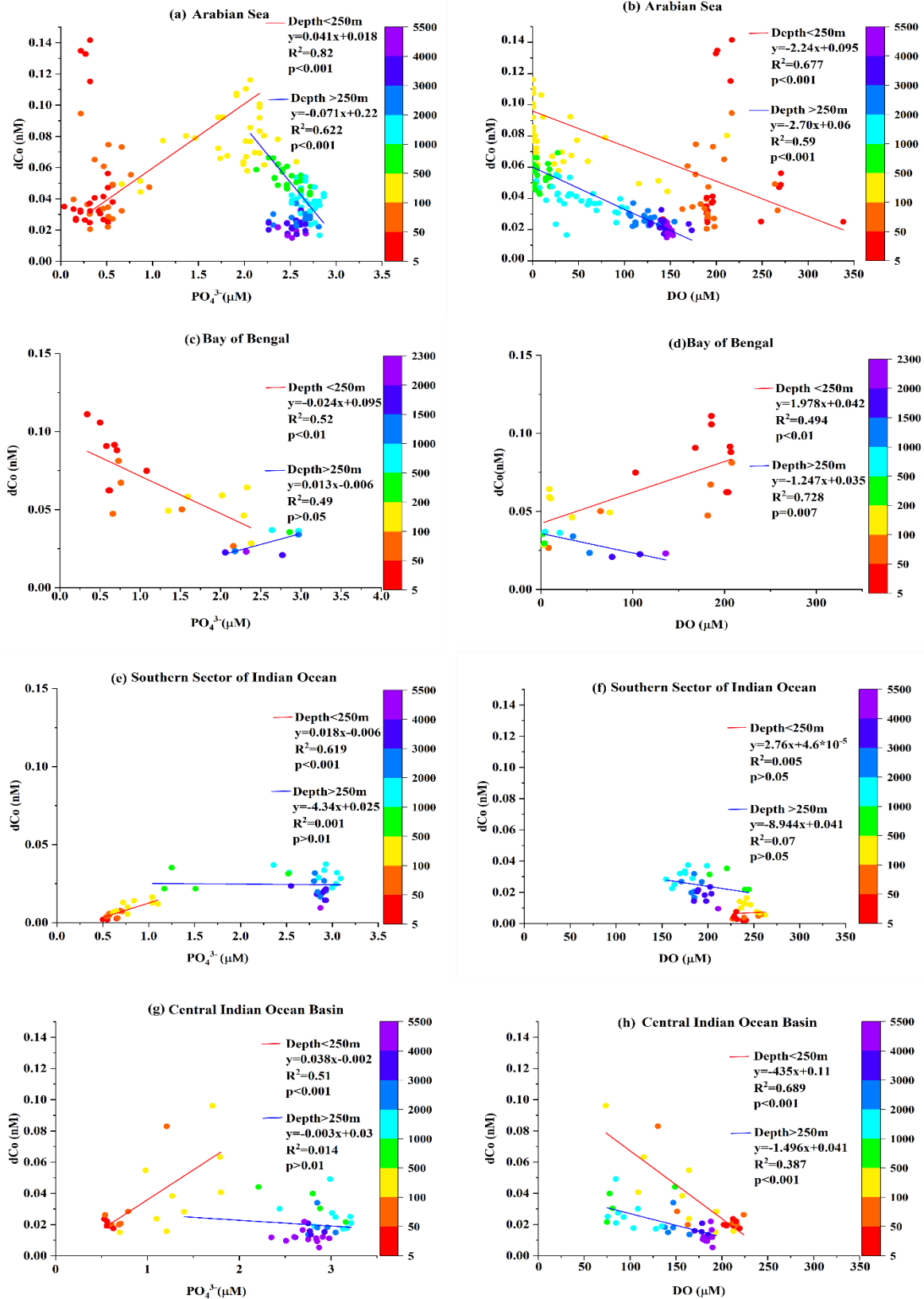


Figure 6: dCo vs PO_4^{3-} and dCo vs DO plots in the water column of different regions of the Indian Ocean (a-b) Arabian Sea (c-d) Bay of Bengal, (e-f) Southern sector of the Indian Ocean, (g-h) Central Indian Ocean Basin. The different depths are colour coded and mentioned in the colour bar. The correlation of dCo with PO_4^{3-} and DO along with regression line and p-value are mentioned in the plots for depths 0-250m (Red line) and >250m (Blue line)

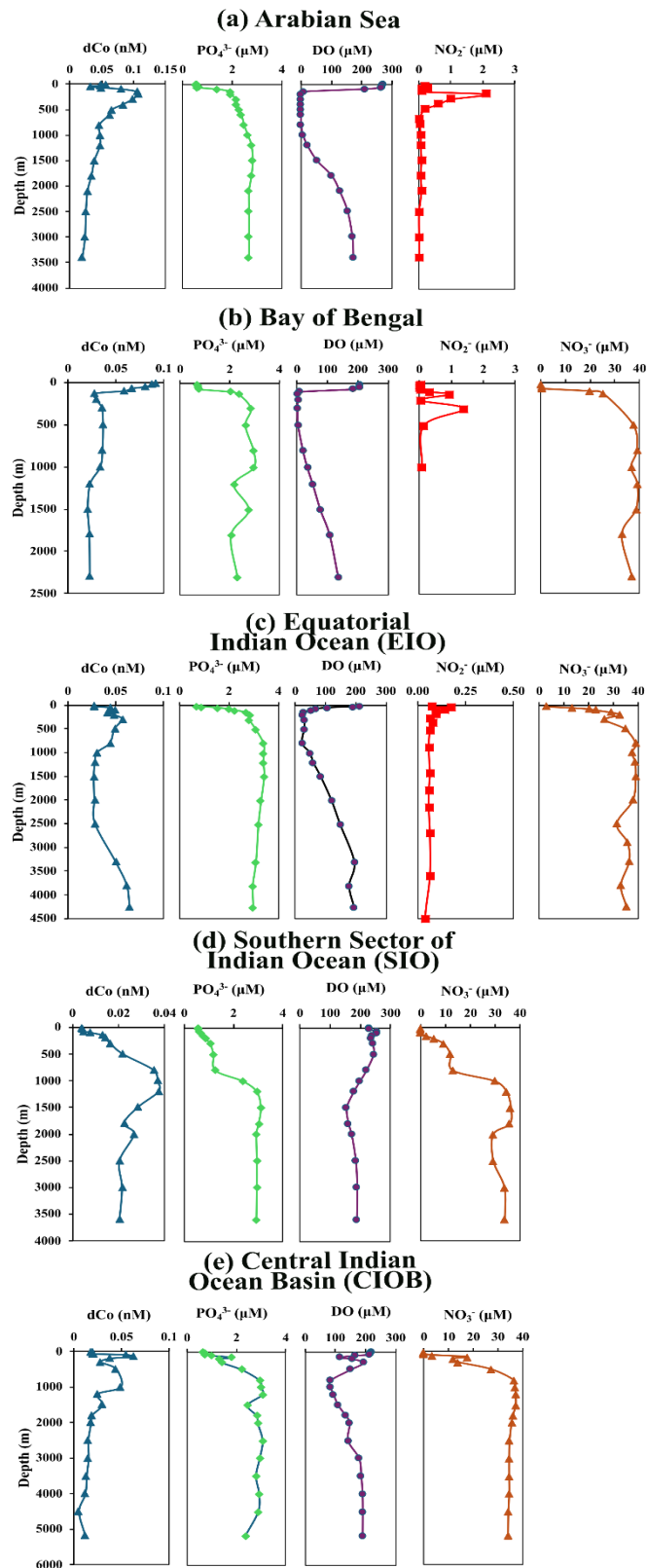


Figure 7: The dCo profile is compared with other chemical parameters like DO, and macronutrients like Silicate, Phosphate, Nitrite and nitrate in different parts of the Indian Ocean. The profile are the representatives for specific regions in the Indian Ocean (Arabian Sea- GI10/17, Bay of Bengal- GI09/02, Equatorial Indian Ocean EIO (GI09/05), Southern Sector of Indian Ocean (SIO)-GI09/15 and Central Indian Ocean Basin (CIOB) - GI09/20). Nitrate could not be measured in the GI10 cruise due to technical issues and Nitrite was not detected in SIO and CIOB.

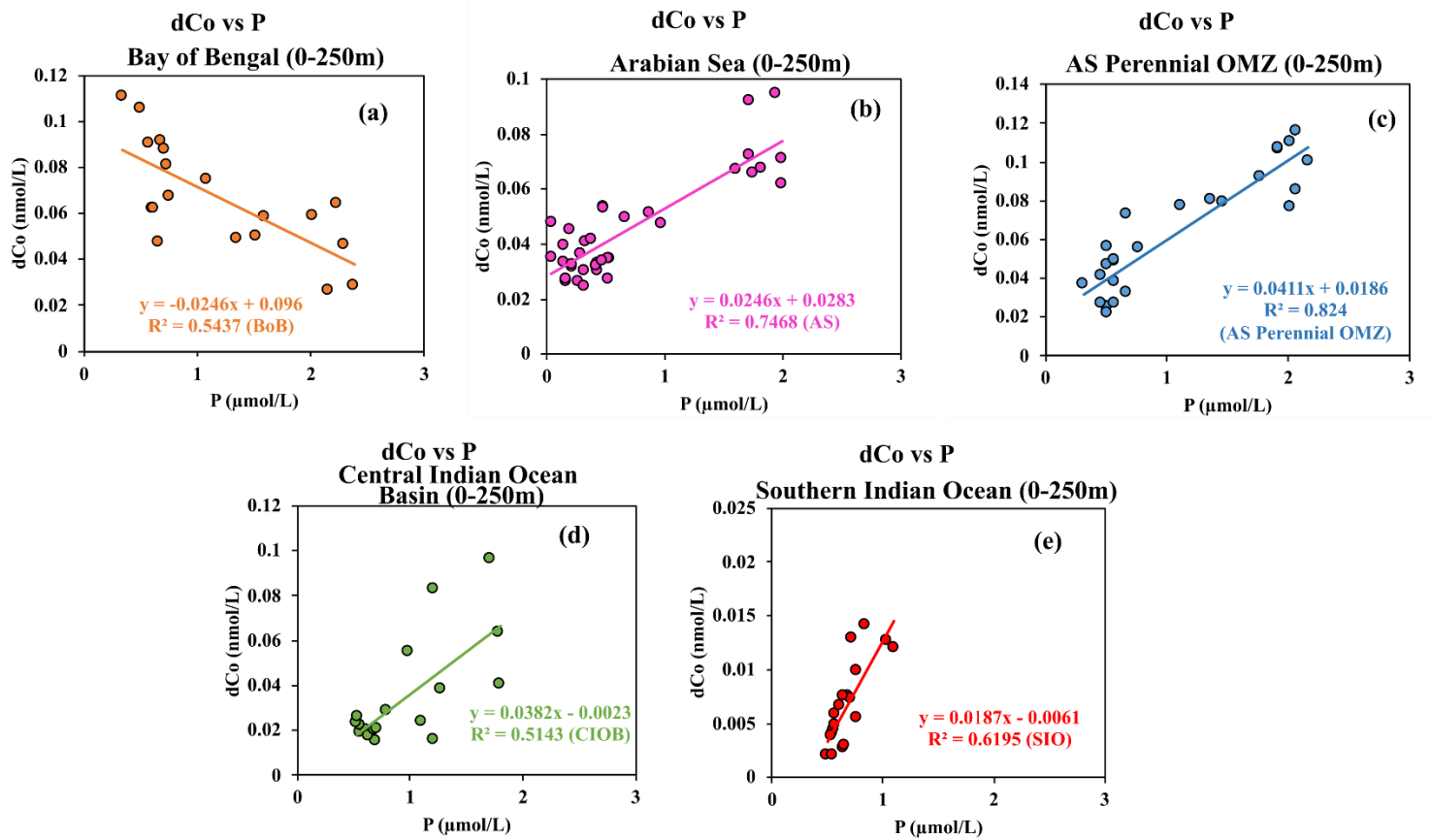


Figure 8: Scatter plots of dCo (nmol/L) and phosphate (μmol/L) in the water depth of 0 -250 m in different parts of Indian Ocean: (a) Bay of Bengal (BoB)- Orange, (b) , Arabian Sea (9°N)- Pink , (c) Arabian Sea Perennial OMZ (ASOMZ)- Blue, (d) Central Indian Ocean Basin (CIOB)- Green and (e) Southern sector of Indian Ocean (SIO)- Red. The slopes, intercepts, and correlation coefficients are mentioned in the plot.

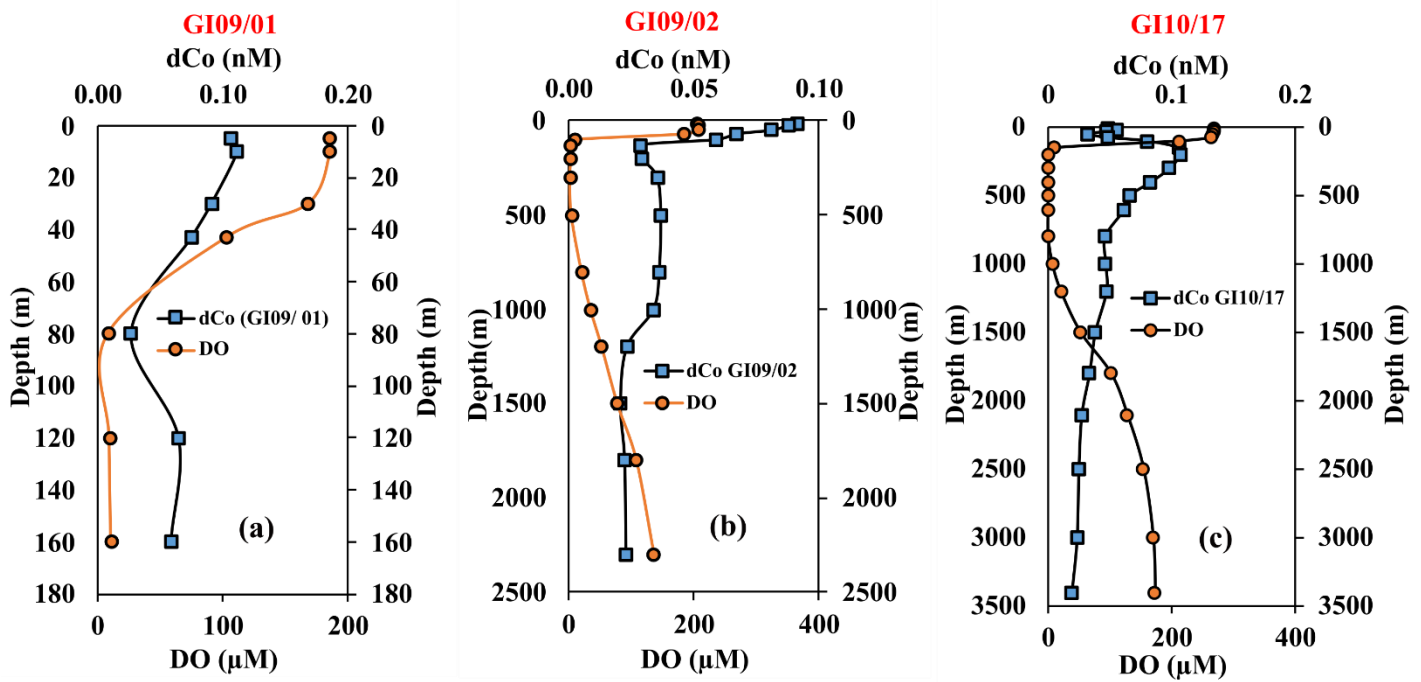


Figure 9: dCo vs DO in the water column (a), (b) in the Bay of Bengal (c) in the Arabian Sea. These profiles show the release of dCo to the water column in low oxygen conditions. Still, the dCo in the OMZ waters of the Bay of Bengal and the Arabian Sea behaves differently due to different biogeochemical processes.

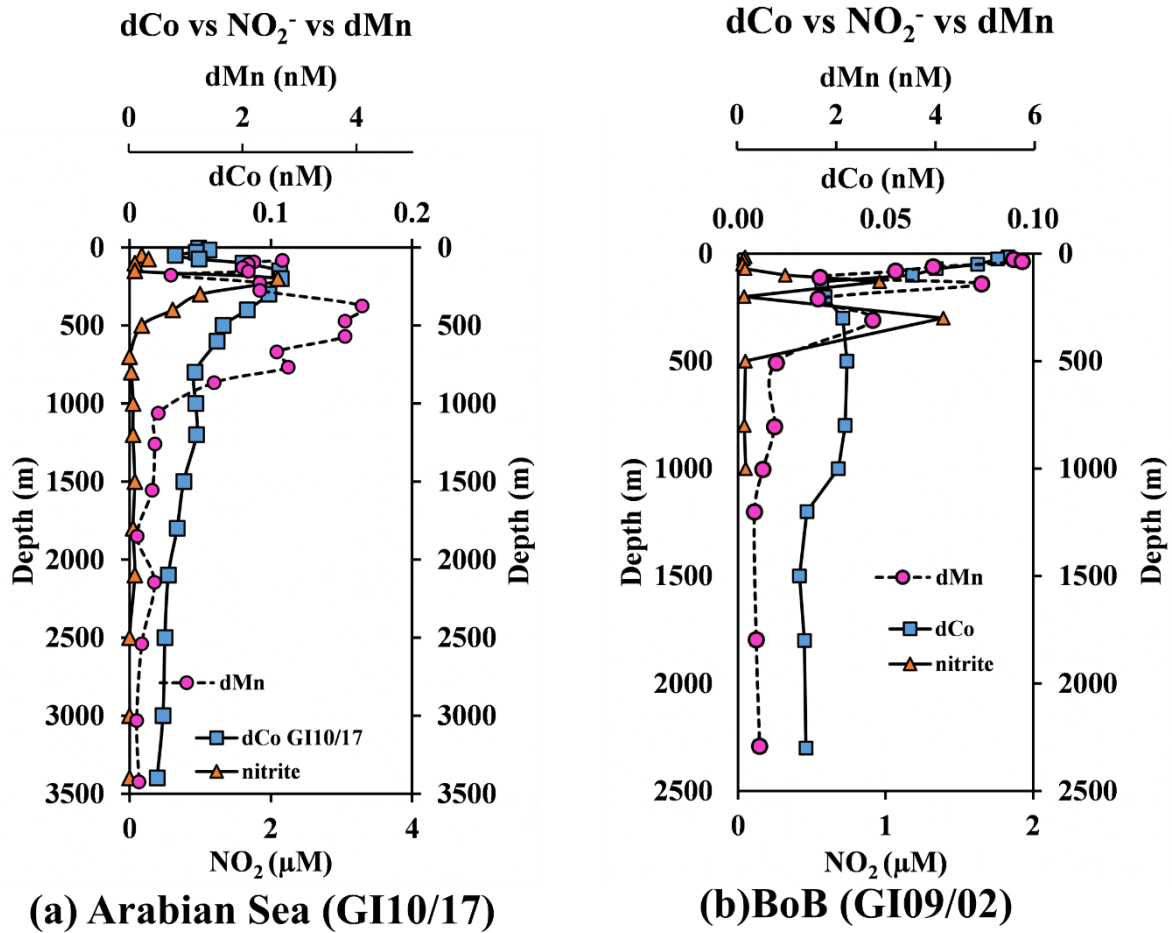


Figure 10: dCo vs Nitrite (NO_2^-) vs dMn in the water column (a) Arabian Sea (b) Bay of Bengal. The dCo in the Arabian Sea is correlated with the nitrite as well as the dMn peak in the zone of denitrification due to the release of dCo and the dMn from the bacterially mediated Mn oxides. However, the dCo is not correlated with the nitrite in the Bay of Bengal. The dMn data of the Arabian Sea (a) is taken from Singh et al., 2023 and that of Bay of Bengal (b) is unpublished data from GI09 cruise.